

Review

Single-Top Quark Physics at the LHC: From Precision Measurements to Rare Processes and Top Quark Properties

Jérémie Andrea¹  and Nicolas Chanon^{2,*} ¹ CNRS, IPHC UMR7178, Université de Strasbourg, 67000 Strasbourg, France; jeremy.andrea@cern.ch² CNRS/IN2P3, IP2I Lyon, University Claude Bernard Lyon 1, 69622 Villeurbanne, France

* Correspondence: nicolas.pierre.chanon@cern.ch

Abstract: Since the initial measurements of single-top quark production at the Tevatron in 2009, tremendous progress has been made at the LHC. While LHC Run 1 marked the beginning of a precision era for the single-top quark measurements in some of the main production mechanisms, LHC Run 2 witnessed the emergence and exploration of new processes associating top quark production with a neutral boson. In this paper, we review the measurements of the three main production mechanisms (t -channel, s -channel, and tW production), and of the associated production with a photon, a Z boson, or a Higgs boson. Differential cross-sections are measured for several of these processes and compared with theoretical predictions. The top quark properties that can be measured in single-top quark processes are scrutinized, such as Wtb couplings and top quark couplings with neutral bosons, and the polarizations of both the W boson and top quark. The effective field theory framework is emerging as a standard for interpreting property measurements. Perspectives for LHC Run 3 and the HL-LHC are discussed in the conclusions.

Keywords: top quark; single-top quark production; top quark properties; ATLAS; CMS; LHC

Citation: Andrea, J.; Chanon, N. Single-Top Quark Physics at the LHC: From Precision Measurements to Rare Processes and Top Quark Properties. *Universe* **2023**, *9*, 439. <https://doi.org/10.3390/universe9100439>

Academic Editors: Efe Yazgan, Pedro Ferreira da Silva and Máté Csanád

Received: 25 July 2023

Revised: 14 September 2023

Accepted: 17 September 2023

Published: 30 September 2023



Copyright: © 2023 by the authors. Licensee MDPI, Basel, Switzerland. This article is an open access article distributed under the terms and conditions of the Creative Commons Attribution (CC BY) license (<https://creativecommons.org/licenses/by/4.0/>).

1. Introduction

After the discovery of the top quark [1,2] in 1995 at the Fermilab Tevatron, the CERN LHC era opened up many opportunities to investigate top quark processes. Both at the LHC and the Tevatron, the processes with the largest cross-sections for producing top quarks in proton–proton or proton–antiproton collisions are the $t\bar{t}$ production modes. In addition to the $t\bar{t}$ production, which arises from quantum chromodynamics (QCD) interactions, top quarks can be singly produced through electroweak interactions. This leads to the so-called single-top quark channels. The single-top quark production features many interesting properties owing to the V–A structure of the electroweak interaction. It shows specific sensitivities to parton density functions (PDFs), the V_{tb} matrix element of the CKM matrix, Wtb coupling beyond the standard model (SM), and top quark polarization, to name a few examples. Measuring inclusive cross-sections and differential cross-sections for single-top quark processes serves as an interesting test of perturbative QCD (pQCD). The associated production of a single-top quark with a boson offers insights into the coupling between the top quark and bosons, complementing the associated production of a boson with a $t\bar{t}$ pair.

Three main production modes for single-top quark processes can be distinguished: production via the exchange of a virtual W boson in the t - and s -channels, and the associated production with a W boson (tW production). The corresponding diagrams in the leading order (LO) in pQCD are presented in Figure 1.

The first observation of single-top electroweak production (t - and s -channels combined) made at the Tevatron [3,4] in 2009, followed by the observation of the t -channel [5]. The CDF and D0 collaborations performed simultaneous measurements of the s - and t -channel processes [6,7]. The $p\bar{p}$ collisions at the Tevatron provided a unique setting for measuring the s -channel since the initial state of this process predominantly involves a

light quark and a light antiquark, taken from the valence partons in the proton and antiproton. To date, the s -channel has been observed solely at the Tevatron [8]; it remains to be observed at the LHC, although there have been reports suggesting evidence of this process at both 8 TeV [9] and 13 TeV [10]. At the LHC, the largest cross-sections at $\sqrt{s} = 13$ TeV (the center-of-mass energy of Run 2) are obtained for the t -channel ($214.2^{+4.1}_{-2.6}$ pb at NNLO with MCFM [11]), followed by the tW production ($79.3^{+2.9}_{-2.8}$ pb at NLO+NNLL [12]), and the s -channel ($10.3^{+0.4}_{-0.4}$ pb at NLO with Hathor v2.1 [13,14]).

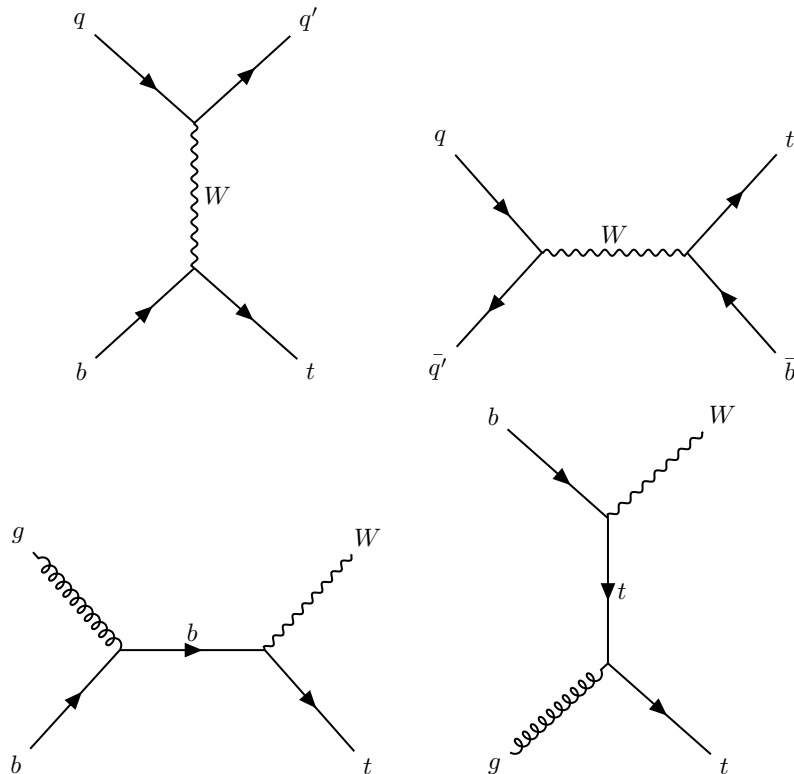


Figure 1. Examples of Feynman diagrams for single-top production at LO: t -channel (top left), s -channel (top right), and tW production (bottom).

At the LHC, many new processes involving single-top quarks were measured in p-p collisions. The t -channel production has been frequently measured and has been thoroughly investigated by evaluating differential cross-sections. Most of the top quark properties probed with single-top production channels are measured using the t -channel production since it yields the largest cross-section at the LHC among all the production mechanisms. The LHC is able to observe the associated tW production, for which the differential cross-sections are even measured. This channel is of particular interest because at next-to-LO (NLO) in pQCD, it features interference with the $t\bar{t}$ process. Understanding the nuances of this interference is still a focal point in the field. As noted in an earlier review (Ref. [15]), Run 1 marked the start of a precision epoch in single-top quark measurements for those main production mechanisms. This is ongoing, with remarkable scrutiny focused on the t -channel and tW production.

In addition, single-top quarks can be produced in tandem with neutral bosons. Those processes yield relatively low cross-sections; however, the additional boson in the lepton channel offers invaluable experimental leverage for measuring couplings or searching for new physics. This class of rare processes covers the production of a single-top quark with a photon ($t\gamma$), a Z boson (tZ), or a Higgs boson (tH). For each of these processes, the single-top quark can be produced via the t -channel, tW production, or s -channel, with the boson emitted from a quark line or a W boson exchange. The $t\gamma$ process was observed only at the end of Run 2. There was anticipation for the discovery of the tZ process at the onset of Run

2; nowadays, it is being measured differentially and is utilized for property measurements. The analysis methodology employed in tZ measurements is close to that of the searches for the tH final states. With great similarity in the tH and $t\bar{t}H$ final states and their common sensitivity to the top quark Yukawa coupling, the tH processes constitute a special case and are searched for simultaneously with the $t\bar{t}H$ production. Because of the destructive interference between processes where the Higgs boson emerges from a W boson or from a top-quark line, the cross-section for the tH production is so small that evidence for such processes remains elusive. However, it is already considered in several analyses because of its unique sensitivity to the sign of the top quark Yukawa coupling, which could lead to a large enhancement of its cross-section. When the review in Ref. [16] was published at the outset of Run 2, it signified the dawn of an era where the processes associating the production of a top quark with a neutral boson began to be measured. Run 2 saw the in-depth exploration of these processes, with a particular emphasis on the tZ production.

The cross-sections for all SM top quark processes measured by ATLAS are compared with theoretical predictions in Figure 2. The cross-sections for single-top production ($t + X$) are generally less than those for top pair production ($t\bar{t} + X$). This top pair production acts as a large background in single-top quark searches.

A summary of the cross-section for single-top quark processes as measured at CMS is compared with theoretical predictions and presented as a function of the center-of-mass energy, as seen in Figure 3. It can be observed that the cross-section for the s -channel process does not grow as fast as that of the t -channel process as a function of the energy, which makes the search for the s -channel more difficult with recent LHC runs. The production of a single-top quark associated with a photon or Z boson results in cross-sections that are lower than those observed in the t -channel, s -channel, or tW production.

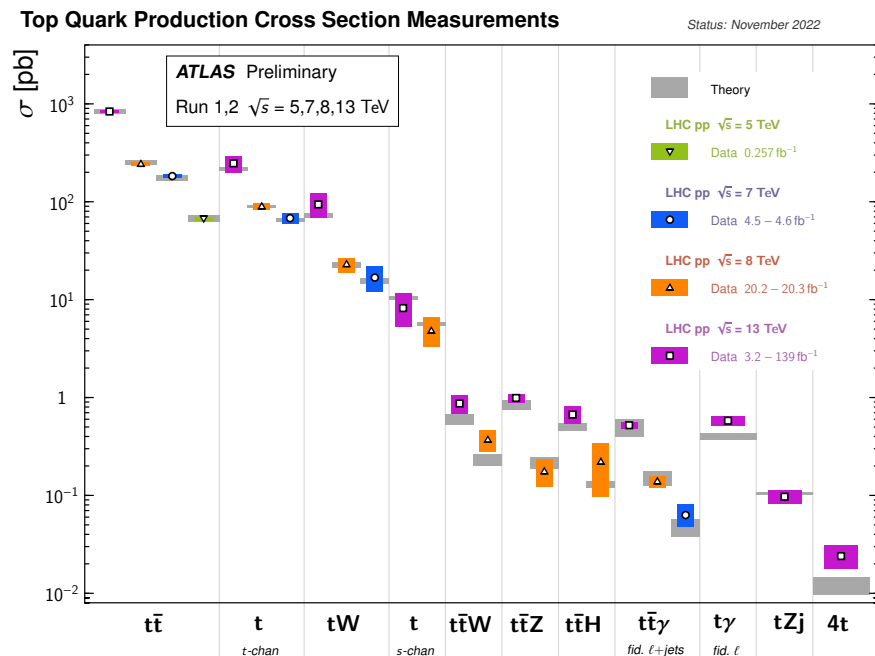


Figure 2. Summary of cross-sections for top quark processes measured by ATLAS [17] and compared with SM predictions.

We will now focus on the top quark property measurements. It is notable that the cross-sections for single-top quark production are directly proportional to the square of $|V_{tb}|$. Therefore, it is possible to determine $|V_{tb}|$ from the measurements of single-top quark

cross-sections. If one assumes that $|V_{td}|, |V_{ts}| \ll |V_{tb}|$, the $|V_{tb}|$ matrix element can be extracted from the following:

$$|V_{tb}| = \sqrt{\sigma_{st}/\sigma_{st}(\text{theo}, |V_{tb}| = 1)}, \quad (1)$$

where σ_{st} is the measured cross-section and $\sigma_{st}^{\text{theo}, V_{tb}=1}$ is the expected cross-section for $|V_{tb}| = 1$. Equation (1) also assumes that no new physics effect modifies the V-A structure of the tWb interaction vertex.

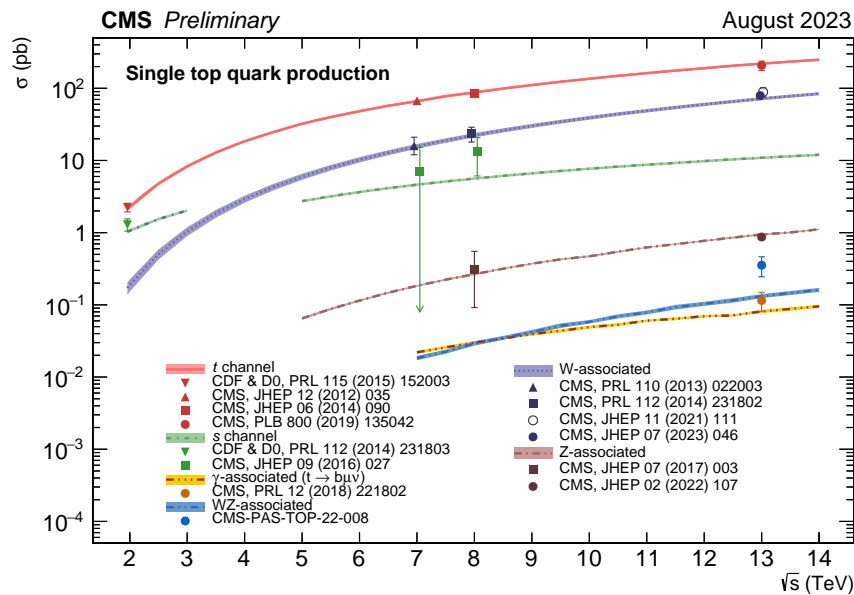


Figure 3. Summary of measured cross-sections for single-top quark production at CMS [18]. Theoretical calculations for the t -channel, s -channel, and W -associated production have been provided by N. Kidonakis to the CMS collaboration.

In single-top quark processes, the Wtb vertex appears in the top quark production and its decay, while in $t\bar{t}$ production, it appears twice in the top quark decay. Therefore, the Lorentz structure of the Wtb coupling can be investigated in detail using decay information. The single-top quark production is also sensitive to the CP property of the Wtb vertex (it is much more difficult to measure in $t\bar{t}$ production, where the CP symmetry is probed preferentially in the top quark–gluon coupling). The W boson polarization and top quark polarization can also be probed. For all of these properties, the t -channel process is usually employed as a probe because of its large cross-section. Within the t -channel, as well as in the associated production with a boson, modern tools, such as the SM effective field theory (EFT), are increasingly used to parametrize deviations from the SM in an almost model-independent way. This systematic approach of searching for signs of new physics is a novelty of Run 2.

The single-top quark production is indeed a sensitive probe in physics beyond the SM. The t -channel signature can occur via the exchange of a supersymmetric particle [19], resulting from the decay of a new heavy resonance, like a color-octet scalar [20] or a new resonance in technicolor models [21]. The s -channel shares the same final state as the possible decay of a W' boson, which is predicted in many models beyond the SM, such as supersymmetric models with R -parity violation [22], or within the paradigm of universal extra dimensions [23]. The tW final state, along with the tZ and tH states, are typical products of vector-like quark decays [24]. Excited top quarks, predicted in Randall–Sundrum models, can decay in the $t\gamma$ final state [25]. The tZ , $t\gamma$, and tH processes can also be modified by flavor-changing neutral currents (FCNCs) in the top quark production or decay, as predicted in several extensions of the SM, like the two-Higgs doublet model [26]

(2HDM), supersymmetry [27], or in warped extra dimensions [28]. In the top quark property domain, for example, CP violation is predicted in the top-Higgs boson coupling within the complex 2HDM [29], and in Wtb coupling within supersymmetric models [30]. The so-called mono-top quark signatures, designating the associated production of a single-top quark with a dark matter candidate, are areas that are being focused on in the quest for new physics (for a review, see [31]).

The outline of this review is as follows. In Section 2, after a brief note on the generation of each single-top quark process, the measurements of the three main single-top quark production mechanisms are presented: t -channel, tW production, and s -channel. The Section 3 will discuss the measurements of single-top quark production in association with a neutral boson (a photon, a Z boson, or a Higgs boson). Top quark property measurements with single-top quark production will be reviewed in Section 4, with a focus on V_{tb} , the W boson, top quark polarization, the structure of the Wtb vertex, and the interpretation in terms of the SM EFT. The conclusions of this review will be presented in Section 5.

2. Precise and Differential Measurements of Single-Top Quark Processes

2.1. The t -Channel Process: The Production Mode With The Largest Statistics

2.1.1. Features of the t -Channel Process

The so-called t -channel production mode features the largest cross-section among all single-top quark production modes. Top quarks produced in the t -channel are accompanied by a high p_T light quark that is predominantly produced in the forward region of the detector ($|\eta| > 2.5$), and of a low p_T b-quark that often fails the minimum jet p_T requirements in the analysis; as a result, it often remains experimentally invisible. Feynman diagrams are presented in Figure 4.

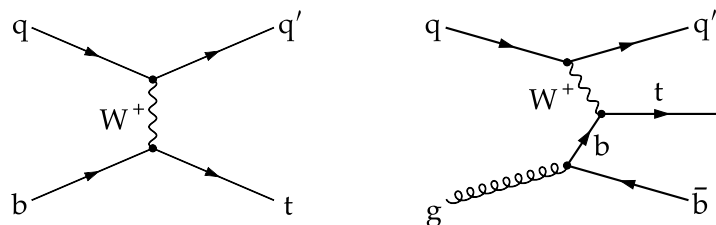


Figure 4. Feynman diagrams for single-top t -channel production at the LO in pQCD [32], in the 5-flavor scheme (left), and 4-flavor scheme (right).

The initial b quark is accounted for in the theoretical calculation according to the 5-flavor scheme (5FS) or the 4-flavor scheme (4FS), as shown in the Feynman diagrams in Figure 4. Each one considers a b quark PDF within the proton (5FS); one can consider that the proton is made of light-flavored quarks in the sea (4FS), in which case, the b quark arises from virtual gluons. In the 5FS, the uncertainty associated with the PDF can be relatively large because b -quark PDFs are not necessarily well known. On the other hand, 4FS calculations usually suffer from higher sensitivity to QCD renormalization and factorization scales. The decision as to whether to employ the 4FS or the 5FS is particularly important for the t -channel signature, where the additional jet (the so-called recoil or spectator jet) is relatively forward, and its pseudorapidity (η) distribution is sensitive to the PDF. It has been observed that the η distribution of the recoil jet ($\eta(j')$) in data is actually better described using the 4FS, while inclusive cross-sections are more accurately described with the 5FS.

With single-top quark production in the t -channel (as well in the s -channel), one of the incoming light quarks can be a valence quark of the proton, depending on whether a top or an antitop quark is being produced. This leads to a larger cross-section for top quark production ($134.2^{+2.6}_{-1.7}$ pb at $\sqrt{s} = 13$ TeV, calculated at NNLO with MCFM [11]) than for antitop quark production ($80.0^{+1.8}_{-1.4}$ pb).

2.1.2. Experimental Techniques for the t -Channel Measurement

The t -channel process was the first single-top production mode observed at the LHC [33,34], thanks to its large cross-section and its manageable signal-over-background ratio. For this channel, clear discriminating observables exist between the signal and background, such as the $\eta(j')$ distribution. Most of the t -channel analyses share a lot of common features in the event selection, background estimation, separation of the signal from the background, and signal extraction. The following paragraphs provide general descriptions of the analysis methods applied in t -channel measurements, and are valid, to a large extent, to the other single-top quark measurements discussed in this paper.

The top quark decays at almost 100% to a W boson and a b-quark. Top quark decays are said to be leptonic ($t \rightarrow bW \rightarrow bl\nu$) or hadronic ($t \rightarrow bW \rightarrow bqq'$). The hadronic decay of top quarks produced in the single-top t -channel leads to a signature with several jets, and suffers from an overwhelming QCD multijet background. For this reason, only the leptonic decay of the top quark is usually studied. The experimental signature for the analysis presented here targets the leptonic decay products from the W bosons: a charged lepton (electron or muon potentially arising from tau lepton decay), and the presence of a significant missing transverse energy \cancel{E}_T originating from a neutrino. Leptons are accompanied by a (mainly) forward light-quark jet and a b-quark jet arising from the top quark decay.

The data sample considered usually selects events with a trigger requiring at least one lepton with a large p_T isolated from hadronic activity. The usage of b-quark identification (“b-tagging”) at the trigger level was investigated in earlier analyses [35], but was found to add a significant complexity for a limited gain, especially with increasing luminosity. To summarize a typical event selection, the presence of only one high p_T -charged lepton (electron or muon with $p_T > 20$ GeV) is required, with a significant missing transverse energy ($\cancel{E}_T > 30$ GeV) and the presence of at least two high p_T jets ($p_T > 30$ GeV), with one of them from a b-quark and the other failing this requirement, while possibly being detected in the forward region ($|\eta(j')| < 4.7$).

The backgrounds can be classified as arising from two main sources: events containing a charged lepton produced from a boson decay (referred to as prompt lepton), and events with hadronic objects misidentified as prompt leptons. Given that prompt leptons are typically distanced from significant hadronic activity while non-prompt leptons are surrounded by hadrons, a potent method to reject the prevalent QCD multijet background is to require the charged lepton to be isolated. An isolation variable is devised by accumulating the hadronic energy around charged leptons, and this needs to be small. As the modeling of a non-prompt background is hardly well-simulated, non-prompt backgrounds are usually estimated directly from the data, possibly leading to large systematic uncertainties. This estimate is performed, for instance, by inverting the lepton isolation requirement, thus enriching the events in QCD multijet processes. The shape of a distribution of interest is then used as a data-driven estimate of the non-prompt lepton background.

The major prompt lepton background events are chiefly from $t\bar{t}$ production with semi-leptonic decays, where jets are not well reconstructed or do not pass the b-tagging requirements. The $t\bar{t}$ process has been extensively studied; precise measurements have been confronted with theoretical predictions. This process is well described by the state-of-the-art Monte Carlo (MC) generators, such that single-top measurements rely on simulations to describe $t\bar{t}$ kinematics, while the normalization is usually estimated or constrained from data.

The associated production of a single W boson with additional jets, referred to as “ W +jets” in the following, constitutes the second main source of background events. The W +jets processes were measured at the LHC, and the event kinematics show a good agreement between data and MC predictions. However, the kinematics of the W +jets process varies slightly depending on the flavor of the additional jets. For this reason, several analyses actually split the W +jets simulation into $W+b$, c , or light jets, measuring the normalization of each contribution separately.

Finally, other subdominant processes after the selection contribute to the background events, such as the Drell–Yan production, when one of the two leptons is not reconstructed or does not pass the lepton selection. These processes are usually estimated from simulations.

The t -channel analyses capitalized on the rise of the LHC profile likelihood method [36,37] to simultaneously estimate the background contributions and constrain the systematic uncertainties from the data. Background normalization is adjusted within the fit, possibly using control regions enriched in background events, usually defined by jet and b-tagged jet multiplicities. For instance, the $t\bar{t}$ background can be controlled by fitting events with at least three jets and two b-tagged jets ($3j, 2t$). The W +jet background can be controlled with events containing two jets and no b-tagged jet ($2j0t$), using the distribution in the transverse mass of the W boson ($m_T(W)$), showing a broad resonance for W bosons, as shown in Figure 5. The signal events are mainly expected in the region defined by asking for two jets, one of which is a b-tagged jet ($2j1t$). The signal is extracted from a combined fit in ($3j, 2t$), ($2j0t$), and the ($2j1t$) regions. Discriminating observables in each of these regions are fitted together with common nuisance parameters representing the systematic uncertainties.

Several distributions can be used to discriminate the signals from backgrounds. In the early versions of analyses, the most obvious observables included the pseudorapidity of the recoiling jet or the reconstructed top-quark mass. In the most precise measurements, the discriminating variables in the ($3j, 2t$) and ($2j1t$) regions are constructed from multivariate analyses, such as boosted decision trees (BDTs) or neural networks (NNs), using various kinematic observables as input. An example is shown in Figure 5. In the latest published cross-section measurement at 13 TeV [32], the BDTs are trained using input variables related to the absolute value of the pseudorapidity of the untagged jet, $|\eta(j')|$, the reconstructed top quark mass, the transverse W boson mass, $m_T(W)$, the distance in the $\eta - \phi$ space between the b-tagged and the untagged jet, $\Delta R(b, j')$, the absolute difference in the pseudorapidity between the b-tagged jet used to reconstruct the top quark and the selected lepton, $|\Delta\eta(b, l)|$.

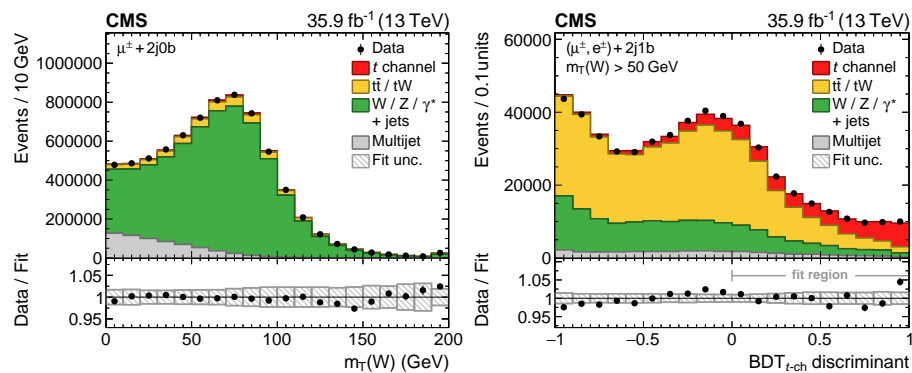


Figure 5. Distribution of the transverse mass of the W boson in the muon channel of the $2j0t$ region (left), the BDT discriminant in the $2j1t$ category (right) [32].

Thanks to the large amount of integrated luminosity collected at the LHC, the uncertainties related to the t -channel measurements are no longer statistically dominated. Remarkably, one can even select a relatively pure sample of t -channel events by applying stringent requirements on the BDT discriminants, as illustrated in Figure 6 (taken from [32]), showing the distribution in the cosine of the top quark polarization angle $\cos\theta^*$ in a background-enriched region (with the requirement of $BDT_{t-ch} < 0$) and in a signal-enriched region ($BDT_{t-ch} > 0.7$). The sample can be vastly enriched in signal events while still providing a large event yield.

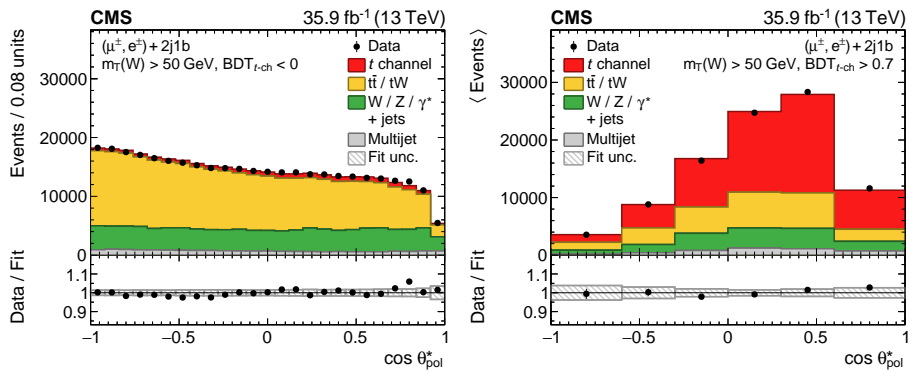


Figure 6. Distributions in the cosine of the top quark polarization angle with a background-dominated selection (left) and a signal-enriched selection (right) for events in the 2j1t region [32].

The main sources of systematic uncertainties impacting t -channel measurements can be summarized as follows:

- Integrated luminosity: Typically a few percent (depending on the dataset).
- Signal and background modeling from SM theoretical predictions: Uncertainties in the modeling of signal acceptance and in the modeling of distributions used as discriminant observables are usually major sources of systematic uncertainty in top quark physics. This includes renormalization and factorization scale variations (accounting for missing higher-order contributions in pQCD), parton shower and hadronization, PDFs, the choice of a matching scheme between fixed-order predictions and the parton shower, the choice of flavor scheme (4FS or 5FS), and MC statistical uncertainty. These uncertainties are treated by generating various MC samples, or including various event weights in the MC samples, with generation parameters varied up and down. The same uncertainties are also included for most backgrounds, which are estimated from simulations.
- Data-driven background estimate: Due to the inadequate representation in simulations of jets misidentified as leptons, the non-prompt lepton background is directly estimated from the data. Usually, these estimations are complicated and rather imprecise. It is rare to lower the relative systematic uncertainty below 30% before any constraints from the fit.
- Simulation-to-data corrections: Several corrections (so-called scale factors) to the reconstructed objects are applied to the simulation to improve its agreement with the data. These corrections are derived from dedicated analyses estimating the associated systematic uncertainties. The corrections are typically related to trigger and lepton selections, jet energy scale and resolution, and b-tagging.

In the most recent analyses, the statistical uncertainty provides a small contribution to the total uncertainty (less than 5%). The relative sizes of the systematic uncertainties depend on the analysis strategy; for instance, the choice of the discriminating observable matters. The use of the $|\eta_{\gamma'}|$ distribution naturally leads to large uncertainties on the jet energy scale and resolution (up to about 5%), since controlling such corrections in the forward part of the detector is difficult. Using a multivariate discriminant can significantly reduce the jet energy scale and resolution uncertainties to a few percent, most likely due to the higher signal purity and increased constraining power. Another large source of systematic uncertainty arises from the signal modeling, which can be lowered by performing a fiducial measurement, as described in Section 2.1.4. Fiducial measurements are performed within a generator-level acceptance to avoid the extrapolation from the visible phase space to the full process phase space, thus reducing the modeling uncertainties.

2.1.3. Summary of the Latest Measurements of the t -Channel-Inclusive Cross-Section

A summary of the latest measurements of the cross-section for t -channel production at $\sqrt{s} = 7, 8$, and 13 TeV from the ATLAS and CMS collaborations can be seen in Table 1,

where the combinations made by the LHCtopWG are also shown when available. Figure 7 shows the relative total uncertainty of the t -channel cross-section $\Delta\sigma_{t\text{-chan}}/\sigma_{t\text{-chan}}$ as a function of the integrated luminosity accumulated at different center-of-mass energies. The most precise 13 TeV measurement was recently released, as a conference note, by the ATLAS collaboration [38]. The t -channel cross-section has also recently been measured at 5.02 TeV by the ATLAS collaboration [39].

In Table 1, it quickly becomes evident that the statistical uncertainty soon turns into a secondary source of uncertainty, with precision measurements primarily dominated by systematic uncertainties. Comparing the most precise result measured at 7 TeV [40] with the published measurement at 13 TeV [41], it becomes clear that while several systematic uncertainties related to detector effects and background estimates have decreased, there is an increase in all the theory uncertainties related to the signal modeling. While experimental systematic uncertainties can be reduced further, a significant improvement in the total precision of the inclusive t -channel cross-section requires effort in the signal modeling involving the theory community. The largest uncertainties that are common to both ATLAS and CMS are related to the parton shower used in the simulation samples of the t -channel and $t\bar{t}$ processes. Sources of large uncertainties can include the choice of the parton shower algorithm, the matching scheme used to interface the NLO fixed-order matrix element with the parton shower, models of hadronization, or final state radiation. Prescriptions should be refined and agreed within ATLAS and CMS (an ongoing effort), and work is needed to decrease the uncertainty based on physics arguments. For instance, improved algorithms, such as antenna-based parton showers, could be tested [42]. The developments of parton showers at NLL [43] or even higher accuracy [44] could bring about large improvements in the future. Eventually, exploring in situ constraints of these uncertainties from ancillary measurements in data [45] is another path to consider.

Table 1. Summary of the most recent and precise t -channel cross-sections from the ATLAS and CMS collaborations, and their combinations for 7 and 8 TeV.

	Cross-Section (pb)	$\Delta\sigma_{t\text{-chan}}/\sigma_{t\text{-chan}}$
7 TeV		
ATLAS [46]	$68 \pm 2 \pm 8 \pm 1$	0.122
CMS [35]	$67.2 \pm 3.7 \pm 4.6 \pm 1.5$	0.091
Combination [40]	$67.5 \pm 2.4 \pm 5.5 \pm 1.1$	0.090
8 TeV		
ATLAS [47]	$89.6 \pm 1.2^{+6.8}_{-5.9} \pm 1.7$	0.076
CMS. [48]	$83.6 \pm 2.3 \pm 7.1 \pm 2.2$	0.093
Combination [40]	$87.7 \pm 1.1 \pm 5.5 \pm 1.5$	0.066
13 TeV		
ATLAS [49]	$247 \pm 6 \pm 45 \pm 5$	0.185
ATLAS [38]	221 ± 13	0.059
CMS [41]	$207 \pm 2 \pm 30 \pm 5$	0.147

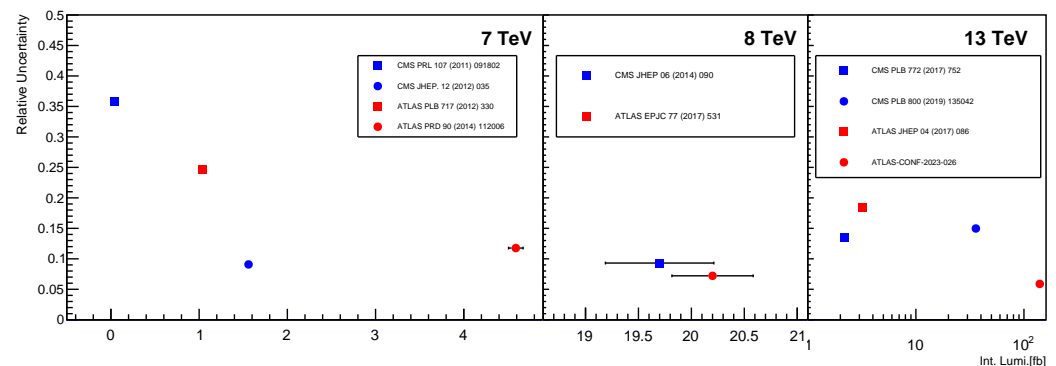


Figure 7. Evolution of the relative total uncertainty in the inclusive t -channel cross-section measurements, plotted as a function of the integrated luminosity at $\sqrt{s} = 7, 8$, and 13 TeV.

2.1.4. Measurements of Fiducial and Differential Cross-Sections

With the latest investigations into the t -channel process, leveraging the extensive statistics of LHC Run 2, differential cross-section distributions [32] were measured. Differential cross-sections provide precious information on the theory modeling, and can also be used to constrain the parameters of the EFT. Differential measurements are critical for a deeper understanding of the t -channel process and for identifying any deviations from SM predictions.

The distributions measured at the reconstructed level are unfolded to theoretically well-defined observables, correcting for detector and acceptance effects. The basic principle consists of determining corrections from simulations to infer the “true” top quark properties, by accounting for the signal acceptance induced by the selection for the detector resolution and the efficiencies. The unfolded distributions can be compared in a robust way with theoretical predictions. Two fundamental unfolding levels are usually defined in top quark physics:

- **Parton level:** Corresponds to the generated on-shell top quarks after QCD radiative corrections.
- **Particle level:** Corresponds to (pseudo-)top quarks reconstructed from simulated particles after QED and QCD radiation, particle decay, and hadronization, with a dedicated algorithm.

With the definitions adopted in [32], measurements unfolded to parton and particle levels are confronted with NLO theoretical predictions for various observables, like the top-quark p_T , rapidity y , $\cos \theta^*$, or W boson p_T . Beyond the differential cross-sections, the charge ratios of the cross-section σ_t to $\sigma_{t+\bar{t}}$ are also measured. This observable is sensitive to the PDFs. Figure 8 presents examples of differential cross-sections and cross-section ratios. The measurements show good agreement between data and NLO predictions, validating our understanding of the electroweak interactions in the production of single-top quarks for most of the observables that were scrutinized. However, the precision reached (even in the differential cross-sections normalized to the total cross-section, thus canceling the impacts of several uncertainties) is not yet completely sufficient to unambiguously determine which generator agrees best with the data. As noted by the authors, a few trends can still be highlighted. The predictions with the 4FS well describe the W boson p_T while the 5FS does not; neither the 4FS nor 5FS predictions are able to nicely reproduce the entire distribution of the top quark p_T in the data. This latter trend can be confirmed with deeper studies in the future since a possible mis-modeling could be of great importance for measurements of top quark properties employing the t -channel, and in measurements or searches in which the SM t -channel is an important background (for instance, the s -channel searches). It should be noted that including t -channel differential distributions in PDF fits allows for reducing the gluon and light quark PDF uncertainties [50]; for this purpose, it is essential to release experimental correlation matrices, which were not made public in the latest measurements.

The so-called fiducial cross-section is defined at the particle level, and is less sensitive than the inclusive cross-section to the systematic uncertainties arising from signal modeling. In inclusive cross-section measurements, the number of signal events is measured in the visible phase space at the reconstructed level, defined by the detector acceptance and selection efficiencies. The observed number of events is then extrapolated to the full phase space based on simulations. This extrapolation induces a large systematic uncertainty related to the modeling of signal events in the simulation. In contrast, the measurement of the fiducial cross-section is performed in the visible phase space, and extrapolated to the fiducial phase space volume that is defined as close as possible to the phase space of the selected dataset. The fiducial single-top t -channel cross-section was measured [47] at $\sqrt{s} = 8$ TeV and led to a reduction of about 2% in the size of the systematic uncertainties related to the QCD scale and the NLO matching. This resulted in a significant improvement in the precision, and provided a robust method for comparing data with theoretical calculations.

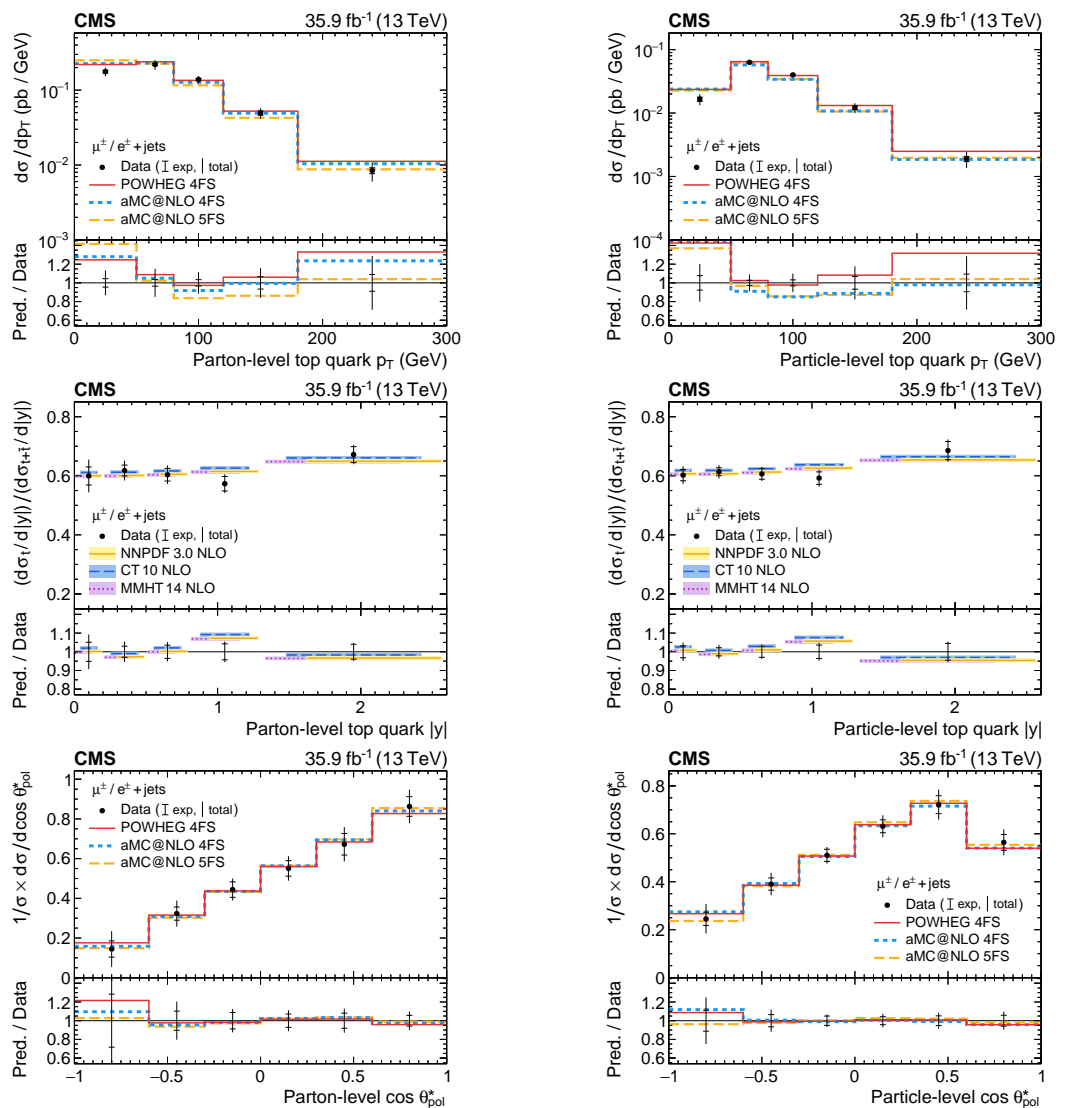


Figure 8. Unfolded differential cross-section measurements: top quark p_T (**upper row**), charge ratio as a function of the rapidity y (**middle row**), and $\cos \theta^*$ (**bottom row**) at the parton level (**left**) and particle level (**right**) [32].

2.2. The tW Process, and Its Interplay with the $t\bar{t}$ Process

2.2.1. Introduction to the tW process

The tW process features a top quark produced in association with a W boson, either initiated by a gluon and a b -quark (in the 5FS, see Figure 9), or with the b -quark produced by gluon splitting (in the 4FS). Because the PDFs for bottom and anti-bottom quarks in the proton in the 5FS are assumed to be the same, the predicted cross-section for tW^- and tW^+ is identical at LO (and almost identical at a higher order) [12].

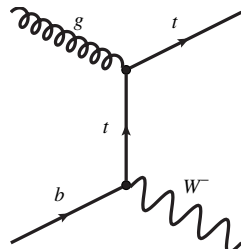


Figure 9. Example of the Feynman diagram for tW production at the LO in pQCD within the 5FS [51].

There is some degree of overlap between the tW process and the $t\bar{t}$ process, since the tW production at NLO in pQCD features resonant diagrams, which interfere with LO diagrams of $t\bar{t}$ production. The NLO corrections to the production of tW include tWb processes, where the Wb system can also arise from the decay of an on-shell top quark. Examples of LO Feynman diagrams for tWb processes are shown in Figure 10. Since the cross-section for $t\bar{t}$ production is much higher than that of tW production, these corrections are very large. As a result, there is ambiguity in the way the $tW + 1$ jet processes are defined. A similar situation is occurring in the FCNC processes [52].

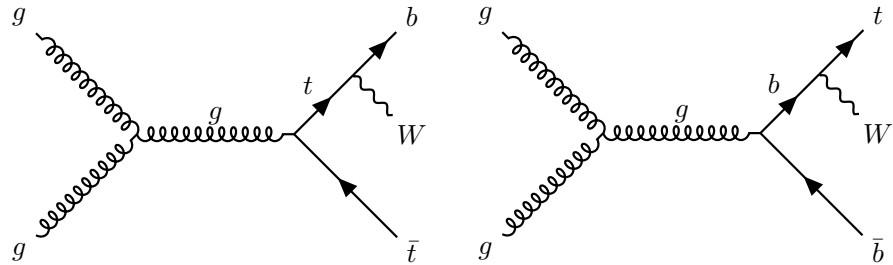


Figure 10. Examples of Feynman diagrams for the production of tWb with (left) and without (right) an on-shell top.

The definition of the tW process, therefore, relies on the treatment of this interference and presents challenges at a theoretical level, depending on the choice of suppressing the interference to define independent simulation samples for the tW process at NLO, or including it in the simulation in a consistent way between tW and the $t\bar{t}$ process. Two methods exist to suppress the interference [53]. In the diagram removal (DR) method, the resonant $t\bar{t}$ diagrams are excluded at the level of the matrix element calculation. In the diagram subtraction (DS) approach, the $t\bar{t}$ resonant contributions are removed from the cross-section calculation by means of counter terms. Thus, a comparison of the DR and DS prediction provides an estimation of the importance of the interference terms and treatment, which is small for the usual kinematic selection applied [54].

2.2.2. Measurements of the tW Process

The tW process has not been measured at the Tevatron, as its cross-section is small at the Tevatron center-of-mass energy in $p - \bar{p}$ collisions. The measurement of the tW process is more challenging than that of the t -channel since a very large background from $t\bar{t}$ events mimics the signal with almost the same experimental signature. The ATLAS and CMS collaborations presented evidence for this process in the dilepton channel at 7 TeV [55,56], while the inclusive cross-section was measured at 8 TeV [57,58] and 13 TeV [59,60]. The measurements at 13 TeV performed with larger collected data samples allowed measuring the differential cross-sections [61,62] for the first time. The tW process was measured in the lepton+jets channel, more difficult owing to larger backgrounds, by ATLAS using 8 TeV collisions [51] and at CMS using 13 TeV collisions [63].

The dilepton decay channel for the tW process refers to processes where one lepton arises from the top quark decay through Wb and another lepton is produced by the associated W boson decay. We describe features of the ATLAS [61] and CMS [62] analyses measuring differential cross-sections at 13 TeV with the dilepton channel, where the leptons refer to electrons or muons. Nominal SM predictions for the tW process use the DR scheme. For this analysis, the main background contribution after event selection is the $t\bar{t}$ process in the dilepton decay channel, amounting to nearly 80% of the event yield after selection. The signal region is defined with exactly one reconstructed jet being tagged as a b-jet (so-called $1j1b$ region) to remove contributions from doubly resonant diagrams. In general, a selection on the transverse missing energy does not need to be applied (among recent measurements, the ATLAS 13 TeV inclusive cross-section measurement [59] is an exception); this variable is used to reconstruct kinematic quantities and provide input to

machine learning techniques. Figure 11 shows the number of events after selection, sorted in bins of the number of jets and b-jets. Two (three) regions that are defined depending on the number of jets and b-jets are used to measure the inclusive cross-section by ATLAS (CMS), with dedicated BDTs.

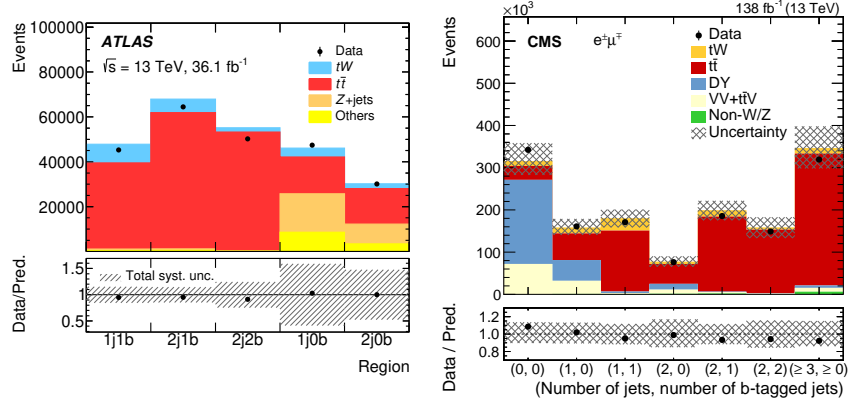


Figure 11. Categories in the number of jets and b-jets in the tW dilepton analysis by ATLAS [61] (left) and CMS [62] (right).

The inclusive cross-section at 13 TeV is measured to be $\sigma_{tW} = 79.2 \pm 0.9 \text{ (stat)}^{+7.7}_{-8.0} \text{ (syst)} \pm 1.2 \text{ (lumi)} \text{ pb}$ at CMS using 138 fb^{-1} [62], and $\sigma_{tW} = 94 \pm 10 \text{ (stat.)}^{+28}_{-22} \text{ (syst.)} \pm 2 \text{ (lumi.) pb}$ by ATLAS using 3.2 fb^{-1} [59], in agreement with SM theoretical predictions. The dominant systematic uncertainty is the jet energy scale, followed by the background normalization and the theory uncertainties on tW process modeling.

The $1j1b$ region—by both ATLAS and CMS—is used to extract the differential cross-sections. In the ATLAS analysis, an additional selection is applied to the output of the BDT to increase the separation between the signal and backgrounds for the differential measurement. In CMS, a veto on additional loose jets is also applied. The data are corrected for detector effects and compared to theoretical predictions, such as the invariant mass of the dilepton and b-jet in Figure 12. In most of the measured bins, the data and simulations agree within less than 1σ ; however, more data are needed to discriminate between the different ways of modeling the signal.

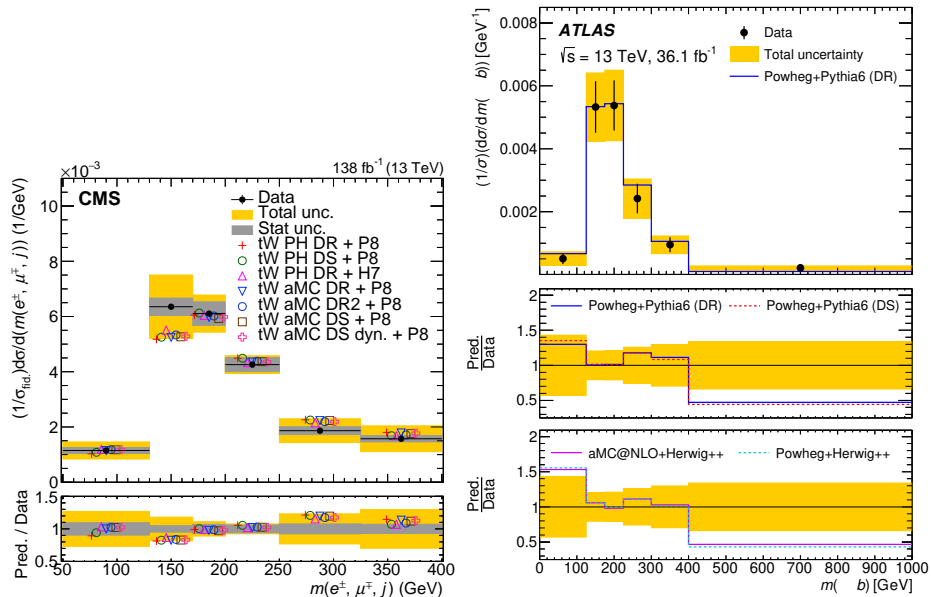


Figure 12. Invariant mass of the dilepton and b-jet in the tW dilepton analysis by ATLAS [61] (left) and CMS [62] (right), comparing data and several predictions for tW modeling.

Measuring the tW process in the lepton+jets channel, which targets a final state where one of the two W bosons decays leptonically and the other hadronically, is a challenging task, owing to the prominent $t\bar{t}$ and W +jet backgrounds arising from the selection. Machine learning methods are used to enhance the signal-over-background ratio, the NN by ATLAS [51], and the BDT at CMS [63]. ATLAS extracts the signal using a two-dimensional distribution in the NN output and the invariant mass of the hadronically decaying W in events with at least three jets (including one b-jet). CMS employs the BDT outputs in three regions, whether there are two, three, or four jets in the event (including one b-jet). The analyses lead to evidence for the tW process in the lepton+jets channel using 8 TeV data by ATLAS, and an observation using 13 TeV data at CMS. The measured inclusive cross-sections are in agreement with the SM predictions, and the precision is already dominated by systematic uncertainties. The main systematic uncertainties arise from the jet energy scale, background normalization, and $t\bar{t}$ or tW modeling.

The lepton+jets analysis shows that, nowadays, more difficult channels are used to measure the tW process. One of the next steps would be to scrutinize the tails of kinematic distributions by using boosted jet tagging, allowing to access highly boosted regions [64,65] that are sensitive to new resonances, like excited b-quarks appearing in theories beyond the SM, such as composite models [66]. Differential distributions are measured with the dilepton channel and will be investigated more differentially in the future. Despite having a smaller cross-section than the t -channel, the tW process could also be used to measure SM parameters. Similar to measurements performed in the t -channel, measuring charge ratios would be interesting since they are sensitive to PDFs; this would require separating top from antitop contributions in tW production with advanced techniques like the matrix element method [67].

2.2.3. Understanding the Interference between tW and $t\bar{t}$ Processes

While the above-mentioned measurements of tW process are designed to minimize the interference with the $t\bar{t}$ process by mostly selecting events with only one b-jet, a recent analysis by ATLAS [68] targeted a phase space with exactly two b-jets, where the interference effect was maximized. This analysis utilized a variable defined as the invariant mass of a lepton and a b-jet as a proxy for the top quark mass. Since there is ambiguity in assigning leptons and b-jets to a given top quark, a particular choice is made:

$$m_{bl}^{minimax} = \min \left(\max(m_{b_1\ell_1}, m_{b_2\ell_2}), \max(m_{b_1\ell_2}, m_{b_2\ell_1}) \right), \quad (2)$$

where particles 1 and 2 are interchangeable. This variable is defined in such a way that, at LO, $m_{bl}^{minimax} < \sqrt{m_t^2 - m_W^2}$. The cross-section above this value has increased sensitivity to the interference between single and double resonant contributions.

Events are selected if there are two leptons and two jets satisfying a tight b-tagging criterion, with a veto on further leptons using a loose requirement (which suppresses backgrounds arising from $t\bar{t}$ associated with heavy flavor jets). The analysis measures the normalized differential cross-section in a phase space at the generator level as close as possible to the reconstructed level, as a function of the $m_{bl}^{minimax}$ observable.

The data are compared to simulations at the particle level in Figure 13, after the background subtraction and correction for detector effects. The simulation sample matching the best data across the entire range of $m_{bl}^{minimax}$ includes both tW and $t\bar{t}$, as well as their interference with POWHEG [69]. Samples featuring interference suppression with the DR or DS scheme do not reproduce the data at large values of $m_{bl}^{minimax}$.

Due to the datasets expected at LHC Run 3 and the HL-LHC, one can expect new measurements to probe the nature of the interference in more depth. The lepton+jets final state could be scrutinized as well for this purpose, since the theoretical predictions at NLO, including the interference, were recently made available [70].

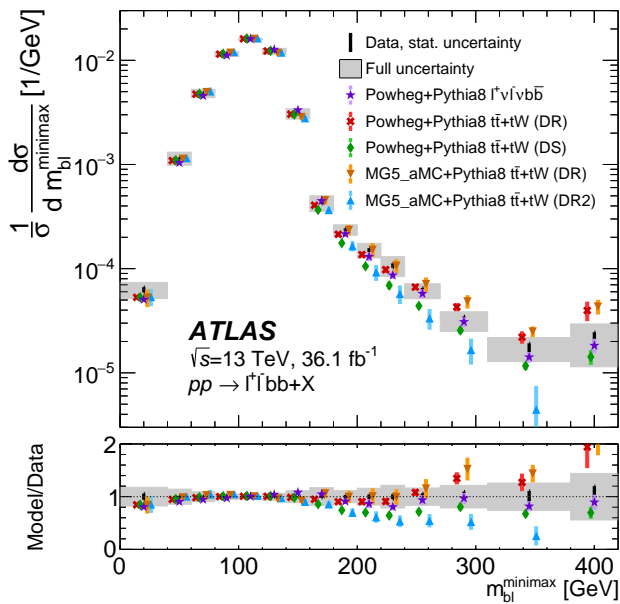


Figure 13. Data comparison of MC predictions for the normalized differential cross-section of the tW process in a region maximizing the interference, as a function of the $m_{bl}^{minimax}$ variable [68]. The region sensitive to the interference lies above $\sqrt{m_t^2 - m_W^2}$.

2.3. The Challenging s -Channel

The final state for top quark production in the s -channel is similar to that of the t -channel in Section 2.1, except that the top quark is now produced with a b or \bar{b} quark in the final state instead of a light quark (in the 5FS). The process occurs through the exchange of a time-like W boson instead of a space-like W boson, as shown in Figure 14. The virtual W boson has to be far away from its resonant mass to produce a top quark, and this highly suppresses the corresponding cross-section, which makes the observation of the s -channel very challenging. The top quark is more likely to be produced with central b -jets than with a forward light jet.

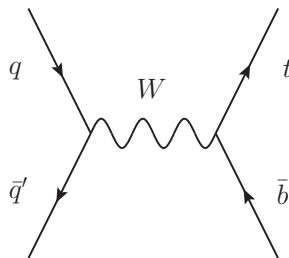


Figure 14. Feynman diagram for single-top s -channel production at the LO in pQCD in the 5FS [9].

The s -channel process is observed at the Tevatron [8], using 9.7 fb^{-1} of proton-antiproton collisions collected at D0 and CDF at $\sqrt{s} = 1.96 \text{ TeV}$. This process remains to be observed at the LHC. At CDF, the lepton+jets channel and $E_T + \text{jets}$ channel are used, while the lepton+jets channel is used at D0. Multivariate techniques are employed to identify the b -jets and reduce the contribution of background processes. Events are classified in categories depending on the number of jets, and the number and quality of b -jets. Multivariate discriminants are built to extract the s -channel cross-section using a Bayesian statistical technique. The result is $\sigma_s = 1.29^{+0.26}_{-0.24} \text{ pb}$, which is in agreement with the SM prediction of $\sigma = 1.05 \pm 0.06 \text{ pb}$ at an approximate NNLO with NNLL accuracy [71] at the Tevatron. The s -channel process was observed at 6.3σ at the Tevatron. Figure 15 shows the measured cross-section for each channel at the Tevatron along with their combined results.

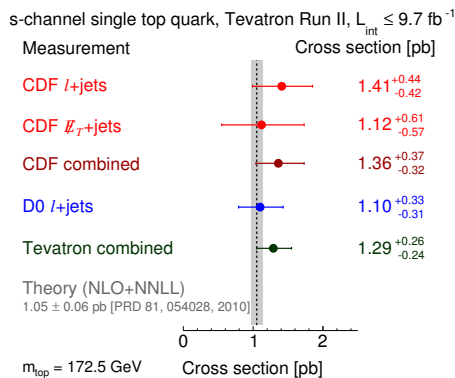


Figure 15. Measured cross-sections for the *s*-channel at the Tevatron along with their combined results [8].

Proton–antiproton collisions at the Tevatron mainly provide a quark and an antiquark in the initial state while the LHC does not. Furthermore, the b-quark content in the proton is larger at the LHC. As a result, the ratio of the *s*-channel to the *t*-channel cross-section decreases from the Tevatron to the LHC. Furthermore, the ratio of signal-to-background is quite favorable at the Tevatron relative to the LHC. When the energy in the p–p center of mass increases, this search becomes more difficult: the quark luminosity increases at a slower pace than the gluon luminosity when increasing the center-of-mass energy. As an example, the ratio of the *s*-channel to the $t\bar{t}$ cross-section changes from 2.1% at 8 TeV to 1.2% at 13 TeV [10].

For all of these reasons, searches for the *s*-channel are very challenging at the LHC. The first search by ATLAS using 8 TeV data resulted in a significance of 1.3σ [72] (with 1.4σ expected); however, a subsequent search on the same dataset employed the matrix element method (MEM [73], which has been used since the early measurements of the top quark mass at the Tevatron [74,75]), leading to an observed significance of 3.2σ [9] (with 3.9σ expected). CMS analyzed Run 1 data using the 7 and 8 TeV datasets, resulting in an observed significance of 2.5σ with an expected significance of 1.1σ [76]. Recently, ATLAS performed a search using the same analysis techniques with the MEM as in their 8 TeV paper, analyzing Run 2 data at 13 TeV [10]. Despite the unfavorable signal-to-background ratio at 13 TeV compared to 8 TeV, a similar observed (3.3σ) and expected (3.9σ) significance was achieved.

Since the ATLAS result is the latest, with the largest observed significance, and the only one published using 13 TeV data, we will provide details on this analysis. The lepton+jet channel is analyzed, with one electron or muon having $p_T > 30$ GeV and at least two jets with $p_T > 25$ GeV. Events from multijet production are reduced by requiring $E_T > 35$ GeV and $m_{T,W} > 30$ GeV. In the signal region, exactly two jets are required, and both of them must be b-tagged. A validation region targets the W +jets process, where one of the jets must fail the b-tag requirement. Events are also validated using two regions enriched in the $t\bar{t}$ process, with three or four jets, among which, two must be b-tagged. The normalization for multijet production is estimated from the data, while the other background processes are taken from the simulation. A dedicated method, the MEM, is employed to further reduce the backgrounds. The MEM consists of calculating a probability density, representing the compatibility of each event with signal and background hypotheses, using exact calculations at the LO in pQCD. Hypotheses for the *s*-channel, *t*-channel, $t\bar{t}$ production, and W boson production are considered. A likelihood is built by combining these hypotheses, and the less likely events are discarded. The shape of the likelihood distribution in the signal region is then used to extract the *s*-channel cross-section. The post-fit distribution is shown in Figure 16, left, and the signal after background subtraction is shown in Figure 16, right. The measured cross-section is $\sigma = 8.2 \pm 0.6(\text{stat})^{+3.4}_{-2.8}(\text{syst})$ pb, in agreement with the SM prediction of $\sigma_{SM} = 10.32^{+0.40}_{-0.36}$ pb at the NLO accuracy in pQCD.

As a side note, predictions at the NNLO in pQCD are available [77] and could be used by the LHC experiments.

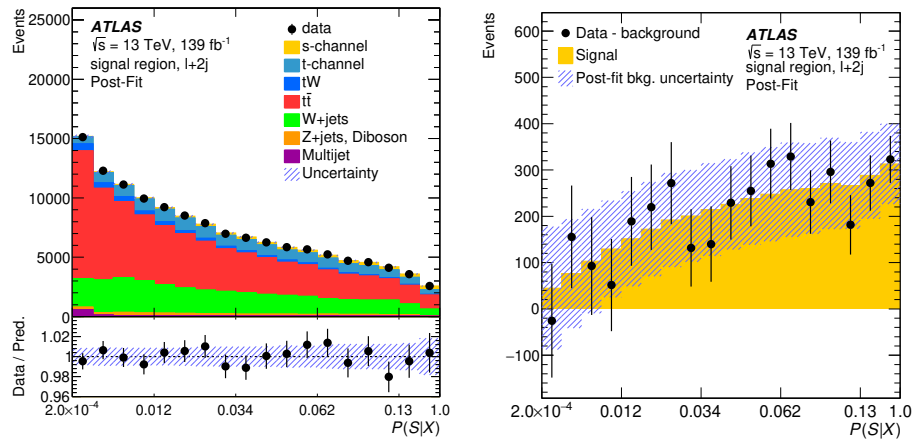


Figure 16. Results of the s-channel searches by ATLAS: (left) post-fit distribution comparing data and simulation for the MEM likelihood, and (right) signal distribution after the background subtraction [10].

As a conclusion, the observation of the s-channel remains to be achieved at the LHC. A result for a CMS analysis using Run 2 data is desired. The analysis is already systematic-dominated; therefore, new techniques should be employed to reduce the uncertainties. A simultaneous fit using signal and control regions could be used to further constrain the background contributions. An involved analysis technique beyond the MEM, like a deep NN (DNN), could also improve the significance. Despite maintaining an unfavorable signal-to-background ratio compared to the Tevatron, the searches should be pursued at the LHC with Run 3 data and at the HL-LHC to make an observation.

3. Associated Production of a Single-Top Quark with a Neutral Boson

3.1. A Newcomer: Associated Production of a Single-Top Quark with a Photon ($t\gamma$)

The production of a photon in association with a top quark ($t\gamma$) is a rare process, accessible at the LHC. The cross-section predicted at NLO in pQCD with Madgraph5_aMC@NLO [78] is $2.95 \pm 0.13(\text{scale}) \pm 0.03(\text{pdf}) \text{ pb}$ (as quoted by CMS [79]), requiring the photon p_T to be greater than 10 GeV before the top quark decay in the 5FS. The cross-section is dominated by t -channel diagrams with the radiation of a photon ($t\gamma q$), featuring a forward jet due to the electroweak nature of the t -channel. The cross-section for the $t\gamma q$ production is known at the approximate NNLO [80]. Measuring the $t\gamma$ process extends the landscape of the measured top quark process and is an experimental challenge, owing to its low cross-section. The $t\gamma$ final states are also powerful tools used to constrain the FCNC [52]. Together with $t\bar{t}\gamma$ processes, they can be used to constrain the top- γ coupling. Examples of Feynman diagrams are shown in Figure 17. The photon can be emitted in the initial state, final state, or in the top quark decay.

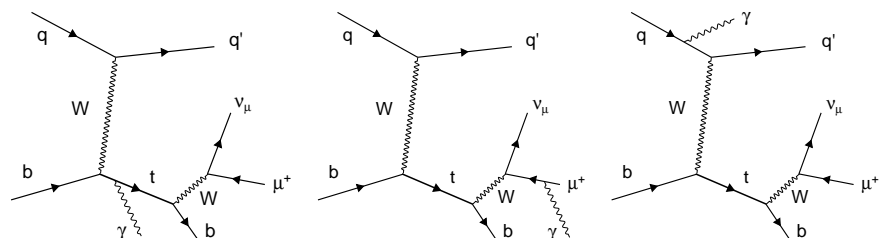


Figure 17. Examples of Feynman diagrams for $t\gamma q$ processes at the LO in pQCD [79].

The searches for the $t\gamma q$ process led to evidence at CMS [79] using 36 fb^{-1} of Run 2 LHC data, and an observation by ATLAS with the full Run 2 dataset [81]. Special care is needed in single-top t -channel MC samples to remove photons produced in the parton shower since they could be double-counted with photons produced at the matrix element level in the $t\gamma q$ signal samples. There is also some freedom in the signal definition: photons arising from the top quark decay are treated as backgrounds in the ATLAS analysis [81]. The dominant backgrounds contain prompt leptons and photons, like $t\bar{t}\gamma$ and $W + \gamma$ processes, and processes involving jets or electrons misidentified as photons (hereafter denoted as “fake photons”). A control region is defined to measure the $t\bar{t}\gamma$ background. The $W + \gamma$ process also benefits from a control region in the ATLAS analysis. The fake photon backgrounds are two-fold, either arising from the misidentification of an electron as a photon, or of a jet as a photon. In the ATLAS analysis, both are estimated with dedicated methods from the data, while in the CMS analysis, only the backgrounds made of jets misidentified as photons are estimated from the data. To maximize the sensitivity to the signal, the signal extraction is performed by constructing a discriminant with a BDT (CMS) and a DNN (ATLAS). Both analyses make use of the forward jet to discriminate the signal against the backgrounds, including the pseudorapidity as an input variable to the machine learning algorithm. The discriminants are shown in Figure 18.

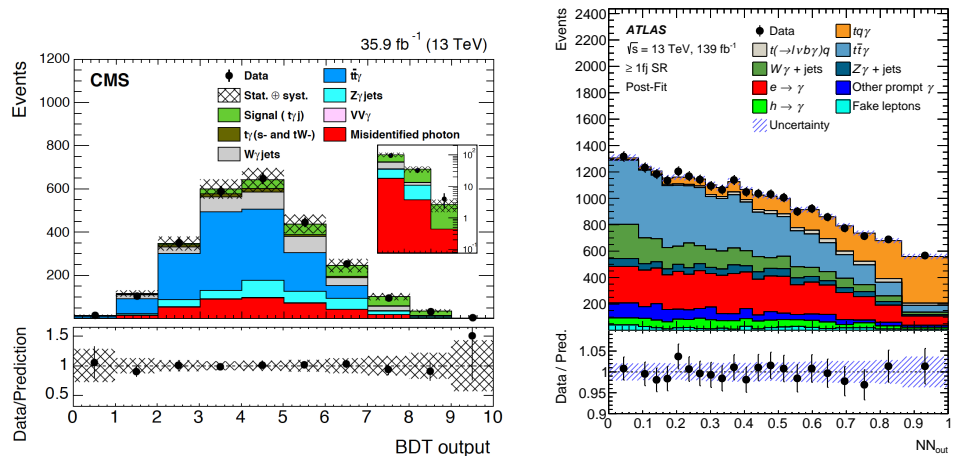


Figure 18. Discriminants used in the $t\gamma q$ signal extraction: BDT output at CMS [79] (**left**) and DNN output by ATLAS [81] (**right**) in the signal region with one forward jet.

The observed (expected) significance obtained is 4.4σ (3.0σ) at CMS [79] and 9.1σ (6.7σ) by ATLAS [81]. With such a large significance, the $t\gamma$ processes can provide sufficient statistics for a first differential cross-section measurement at LHC Run 3. Complementing the $t\bar{t}\gamma$ channel with the $t\gamma q$ channel to probe the top-photon coupling will become especially relevant at the HL-LHC [82]. As a side note, the single-top $tW\gamma$ process has also been measured simultaneously with the $t\bar{t}\gamma$ process [83] because of the interference at NLO, similar to the tW and $t\bar{t}$ processes, but in a $t\bar{t}\gamma$ phase space chosen without particular enhancement of the $tW\gamma$ process or the interference.

3.2. A Path toward Top-Z Coupling: Single-Top Quark Production with a Z Boson (tZ)

The first process observed for single-top quark production in association with a neutral boson is actually the single-top quark production with a Z boson (tZ), due to the datasets made available at the LHC. In general, the tZ processes refer to the production of a single-top quark in association with a Z boson, including the interferences between on-shell and off-shell γ^* or Z bosons. Similar to the $t\gamma$ process, the process with the largest cross-section is provided in the t -channel (tZq).

The Feynman diagrams for tZq production at the LO in pQCD can be seen in Figure 19. The inclusive tZq cross-section predicted at NLO in the SM, as calculated with MG5_aM@NLO, is $800 \text{ fb}^{+6.1\%}_{-7.4\%}$ [84]. Because of its clear signature and interesting signal-to-background

ratio, the tZq process is measured in the three-lepton channel. The cross-section for tZq production in the three-lepton decay channel, calculated at NLO with MG5_aMC@NLO, and including a dilepton invariant mass cut of $m_{\ell\ell} > 30 \text{ GeV}$, is $94.2^{+1.9}_{-1.8}$ (QCD scale) ± 2.5 (PDF) fb [85]. The cross-section for tZq production could be updated with the latest predictions at the approximate NNLO [86] in future measurements.

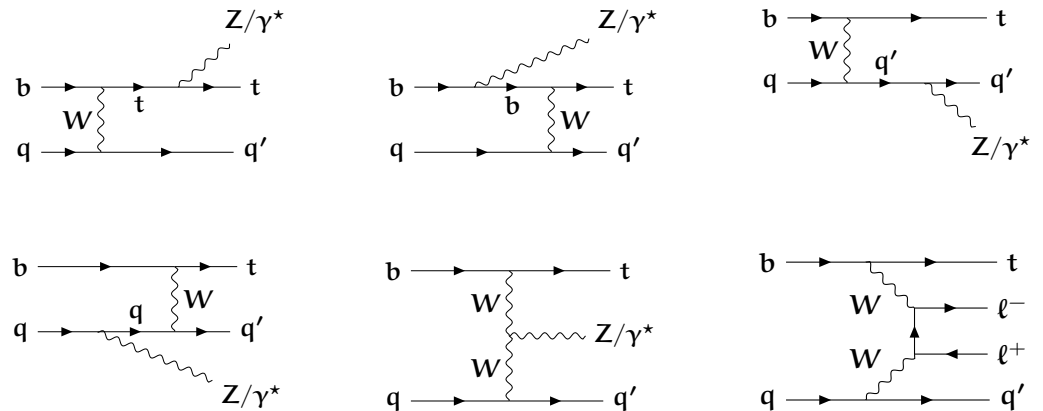


Figure 19. Representative Feynman diagrams for the tZq production at the LO in pQCD [87].

The tZq production has several interesting features. In a similar way with the t -channel process without an associated Z boson, the top and antitop quarks from the tZq production are strongly polarized, making this process an excellent probe for studying $t - Z$ couplings, particularly in the context of EFT measurements. It is also sensitive to triple-gauge couplings WWZ , in a complementary manner with the diboson production. Both are potentially sensitive to physics beyond the SM.

Data are selected with a combination of single-lepton or double-lepton triggers. Events are selected events if they contain three well-identified and isolated leptons (electrons or muons possibly arising from τ lepton decays). A pair of same-flavored opposite-charged leptons, compatible with a Z boson decay, is then required. Because the tZq process is a t -channel process, it contains a light jet preferentially produced at large $|\eta|$, a b-tagged jet arising from the top quark decay, and missing transverse energy arising from the neutrino from the W boson decay.

Similar to other analyses presented in this review, the signal is extracted from signal and control regions defined by the number of jets and b-tagged jets. The first signal region requires $N_j = 2$ or $N_j = 3$ with $N_b = 1$ (so-called $2j1b$ and $3j1b$ regions). These regions contain most of the signal with the $WZ + \text{jets}$ process as the dominant background, and with contributions from other diboson processes. For larger jet multiplicities and b-tagged jet multiplicities ($N_j \geq 3$, $N_b \geq 2$), the dominant background source arises from $t\bar{t}Z$ events, with contamination from $tt + W, H$ processes. A control region with $N_b = 0$ allows constraining the diboson contribution.

Other background sources are from non-prompt lepton events in $t\bar{t}$ or $Z + \text{jets}$ processes. While backgrounds presenting three prompt leptons are estimated from simulations and constrained from the data in the likelihood fit, events containing at least one non-prompt lepton are not well-described by simulations and are, therefore, more difficult to estimate. In the CMS observation paper [88], the analysis uses a fully data-driven technique, where the probabilities for measuring a non-prompt lepton are measured from a region where one lepton fails the lepton isolation. The ATLAS observation paper [89] uses a semi data-driven technique, where the normalization of the non-prompt background is estimated from the data in control regions, and the kinematic distributions are determined from simulations of $t\bar{t} + tW$ and $Z + \text{jets}$ events, by replacing b-jets with non-prompt leptons and accounting for the needed corrections.

The discriminating variables used in the fit are based on multivariate discriminants (BDT or NN), which include kinematic variables related to the reconstructed Z bosons or

top quarks, the pseudorapidity of the spectator jet $|\eta_{j'}|$, dijet invariant mass, or kinematic variables related to the lepton from the W decay. Examples of NN output distributions from ATLAS [89] can be found in Figure 20.

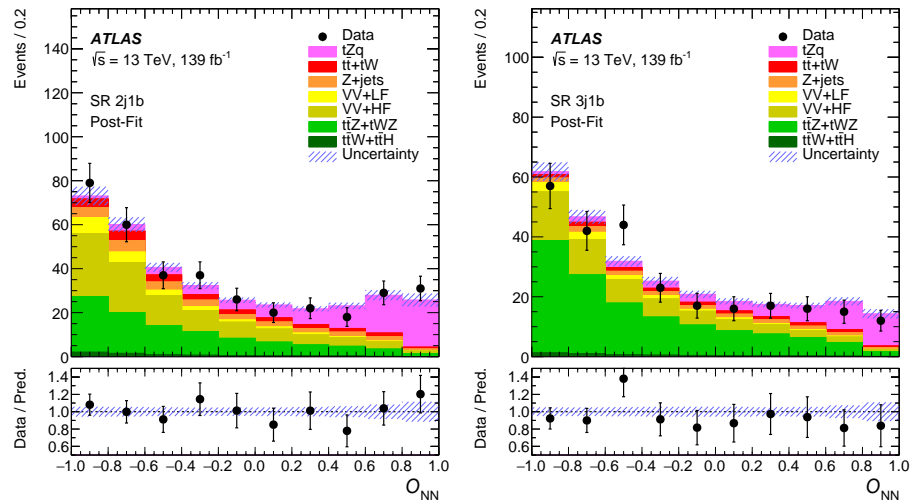


Figure 20. Distributions of the NN output in the signal regions $2j1b$ (left) and $3j1b$ (right) in the ATLAS analysis [89].

The most recent inclusive tZq cross-sections measured by ATLAS [89] and CMS [87] are compatible with the SM. The precision is still dominated by statistical uncertainties, although with the CMS results, systematic and statistical uncertainties are almost of the same level. The dominant sources of systematic uncertainties are mainly experimental, and are not identical between ATLAS and CMS (while the analysis techniques are relatively similar). For ATLAS, the dominant uncertainties arise from background modeling and normalization, the jet energy scale, and the lepton selection; for CMS, the systematic uncertainties are dominated by the QCD scale uncertainties in the signal modeling, non-prompt lepton background estimation, and WZ process normalization. All these uncertainties have similar orders of magnitude. Differences in the relative sizes of the systematic uncertainties by ATLAS and CMS are probably explained by differences in the analysis strategy, noticeably in the treatment of the background estimates.

Due to the large integrated luminosity provided by the LHC, it is now possible to measure differential cross-sections for tZq production [87]. This analysis follows a different approach to extract the signal. A multi-class NN is used to separate the tZq process from the $t\bar{t}Z$, WZ , and other $t + X$ processes. The signal region is then sub-divided based on the bins of the observables of interest, at the detector level. The NN score of the tZq node is used to extract the signal in each bin. Similarly, the NN score of the $t\bar{t}Z$ node is used to constrain the $t\bar{t}Z$ background. An unfolding procedure infers the particle- or parton-level distributions. Examples of differential cross-section measurements for $p_T(Z)$ and $p_T(t)$ at the parton level, and $|\eta(j')|$ and $\cos\theta_{pol}^*$ at the particle level are shown in Figure 21. The $\cos\theta_{pol}^*$ variable is the cosine of the polarization angle of the top quark, defined as:

$$\cos\theta_{pol}^* = \frac{\vec{p}(q'^*) \cdot \vec{p}(l_t^*)}{|\vec{p}(q'^*)||\vec{p}(l_t^*)|} \quad (3)$$

with $\vec{p}(q'^*)$ and $\vec{p}(l_t^*)$, the three momenta of the light jet and the lepton from the top quark decay. A good agreement between data and predictions is observed. This very promising publication presents the first differential measurements of a rare single-top process, and can serve as the basis for future studies. In particular, it provides a clear procedure to perform a differential measurement, featuring an interesting signal extraction based on a multi-class discriminant.

Eventually, the first measurement for the tWZ process led to evidence [90] (presented as a conference note by CMS). This very rare process can be seen as a tZ production in the tW channel, where it shares similar modeling issues since it interferes at NLO with the $t\bar{t}Z$ process [91]. The analysis techniques are similar to those of the tZq analysis, using a multi-class NN, with a multi-lepton signature targeted. This result opens up a new era for measuring top quark processes associated with multi-bosons.

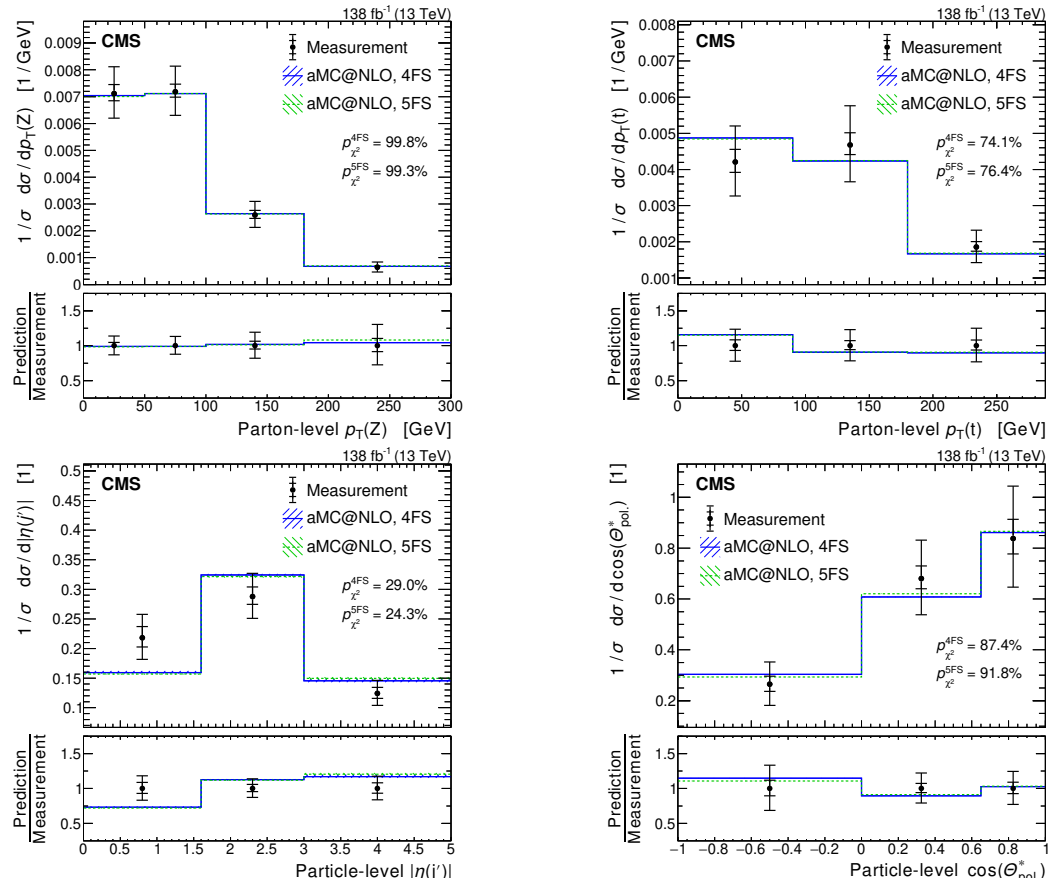


Figure 21. Normalized differential cross-sections measured at the parton level as a function of $p_T(Z)$ (**top left**) and $p_T(t)$ (**top right**) at the parton level, and as a function of $|\eta(j')|$ and $\cos\theta_{pol}^*$ at the particle level [87]. The inner and outer vertical bars represent the systematic and total uncertainties, respectively.

3.3. The tH Processes: Companions for the top Quark Yukawa Coupling

3.3.1. Introduction to the tH Processes

Among the processes involving a top quark and a boson in the final state, the tH processes are produced with the lowest cross-section predicted in the SM, of approximately 71 fb and 16 fb at NLO for the t -channel (tHq process) and the tW -associated production (tHW process) with $\sqrt{s} = 13$ TeV [92]. The latest predictions for the tHq cross-section are computed at NNLO in pQCD [93]. The tHq processes share many properties with the $t\gamma q$ and the tZq processes, noticeably their modeling in the 4FS or 5FS schemes, and the production of an associated quark in the forward direction. The Feynman diagrams for the production of tHq are depicted in Figure 22. The tHW production is also considered in the analyses.

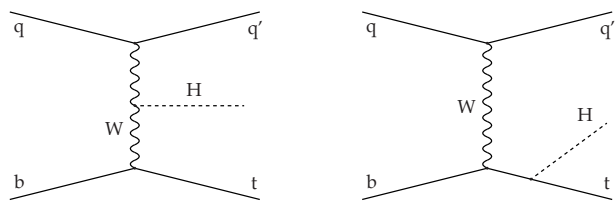


Figure 22. Examples of Feynman diagrams for tHq processes at the LO in pQCD [94].

The search for tH processes is traditionally performed in association with the search for the Higgs boson measurement in the $t\bar{t}H$ production mode, whose cross-section is larger than the cross-section of the tHq process by a factor of 10, as shown in Figure 23. The amplitude for tHq production features an interesting property, as it features interference between diagrams where the Higgs boson is emitted from a top quark line and those arising from W boson exchange. This property makes the measurement of the tHq process appealing since it provides access to the sign of the Yukawa coupling of the top quark. If the sign of the Yukawa coupling κ_t is negative, the interference becomes constructive, for instance, by increasing the cross-section by a factor of approximately 12 if $\kappa_t = -1$ [95]. The tH final states, on equal footing with the tZ and the $t\gamma$ final states, are also used in the FCNC searches [52].

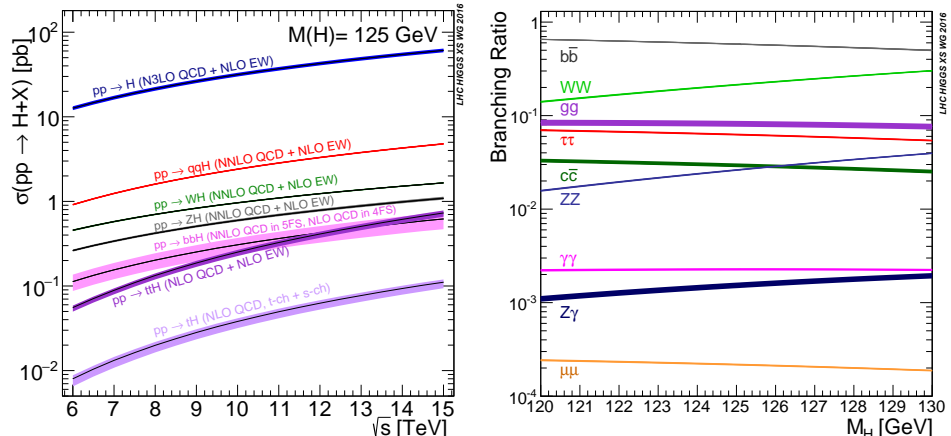


Figure 23. (Right) Cross-section for the Higgs boson production as a function of \sqrt{s} . (Left) branching ratio for the Higgs boson decay [92].

3.3.2. Searches for the tH Processes

The early searches for the tH processes at 8 TeV [94] attempted to directly measure the tH production, while the $t\bar{t}H$ process was treated as a background. It was, however, realized that by varying the value of the top quark Yukawa coupling, the cross-section for both the tH and $t\bar{t}H$ processes would be modified in a correlated way. Nowadays, the searches for the tHq process are performed in a combined measurement with the $t\bar{t}H$ process, either targeting the measurement of the top quark Yukawa coupling or simultaneously measuring the cross-section for the tH and $t\bar{t}H$ processes.

Branching ratios for the Higgs boson decay are shown in Figure 23. The ATLAS and CMS analyses target the main decay modes of the Higgs boson: $H \rightarrow \gamma\gamma$; $H \rightarrow WW$, $H \rightarrow ZZ$, and $H \rightarrow \tau\tau$ (grouped under the naming of the “multilepton final state” since W , Z , τ , and associated top quarks can decay leptonically), and to a lesser extent, $H \rightarrow b\bar{b}$ (suffering from a lack of available luminosity to achieve similar sensitivity as the other channels). We present here the methodology and the latest results.

The analysis of the $H \rightarrow \gamma\gamma$ decay channel with Run 2 data by ATLAS [96] and CMS [97] follows a similar strategy to the measurements of the other production mechanisms of the Higgs boson. The small $H \rightarrow \gamma\gamma$ branching fraction (close to 0.2% at $m_H = 125$ GeV) is compensated by the excellent resolution of the electromagnetic calorime-

ters (the effective mass resolution on the Higgs boson is close to 1.5 GeV, depending on the analysis categories). The background processes involving jets reconstructed as photons are reduced using photon isolation and information on the shape of the electromagnetic energy deposit, with sequential criteria by ATLAS and a multivariate method at CMS. Several event classes are constructed, specifically targeting a given production mechanism. For each event class targeting the tH processes, the background is reduced by the means of a BDT discriminant, which is subsequently fitted with a smoothly falling function. In the latest versions of the analysis [96,97], several subcategories are built to specifically target the $t\bar{t}H$ and tH processes in kinematic bins, and the fit is interpreted in the so-called “simplified template cross-section” framework (STXS) [98]. The STXS framework is a convention used to provide results in kinematic bins at particle levels within a defined acceptance for each Higgs boson production mechanism. In the CMS analysis, a category at the reconstructed level specifically targets tH in the leptonic channel, and a DNN discriminant is used to improve the separation between $t\bar{t}H$ and tH . Using this category, together with many reconstructed-level event classes in a simultaneous fit, the cross-section for the tH processes at the STXS level is quoted to be $6.3^{+3.4}_{-3.7}$ times the SM expectation (in the so-called “maximal merging scenario”, where fewer STXS categories are used at the particle level than in the “minimal merging scenario”). In the ATLAS analysis, four reconstructed categories targeting tH processes are defined, where two categories specifically target the tHq processes with either a positive or a negative top quark Yukawa coupling (defined using the output of a NN), one category targets the tHW process, and the remaining category gathers events with low-scores of the BDT for tHq and $t\bar{t}H$. At the STXS level, the cross-section for the tH processes is $2.1^{+4.2}_{-3.1}$ times the SM expectation.

Using the multilepton channel, CMS [99] reported measurements of the cross-section for $t\bar{t}H$ and tH production simultaneously with Run 2 data. This analysis uses multiple final states. For leptonic top decay, the configurations are the same-sign $2\ell + 0\tau_h$ (where $\ell = e, \mu$ and τ_h denotes hadronically decaying τ), $3\ell + 0\tau_h$, $2\ell + 1\tau_h$ (both same-sign and opposite-sign), $1\ell + 2\tau_h$, $4\ell + 0\tau_h$, $3\ell + 1\tau_h$ and $2\ell + 2\tau_h$. For hadronic top decay, the configurations are $1\ell + 1\tau_h$ and $0\ell + 2\tau_h$. The sensitivity arises mainly from the same-sign channel $2\ell + 0\tau_h$, $3\ell + 0\tau_h$, and $1\ell + 2\tau_h$. In those main categories, the analysis employs a multi-class DNN, separately providing discriminants for $t\bar{t}H$ and tH , while using simpler BDTs in the other categories. In the same-sign channels, $2\ell + 0\tau_h$, $2\ell + 1\tau_h$, categories are further divided according to the lepton flavor and whether the b-jet number is larger or smaller than 2. The jet-faking lepton background is estimated with a data-driven method by relaxing lepton identification criteria in a region enriched in multijet events. Backgrounds resulting from mismeasuring the lepton charge are determined using $Z \rightarrow ee$ events. The dominant background arises from $t\bar{t}W$ and $t\bar{t}Z$ processes, estimated from simulation. The background arising from the conversion of leptons in the detector is estimated from the simulation. The signal is extracted using bins in the multivariate discriminants. Several control regions with 3ℓ and 4ℓ final states are also used in the fit. Two parameters of interest are measured: the signal strength μ for $t\bar{t}H$ and for tH processes. The signal strength for tH production is $5.7 \pm 2.7(\text{stat}) \pm 3.0(\text{syst})$. Additionally, a 2-dimensional distribution of the likelihood as a function of $\mu_{t\bar{t}H}$ and μ_{tH} is measured, as shown in Figure 24.

A few results arising from combinations of final states are also reported. A dedicated CMS analysis specifically targeting tH at 13 TeV using 36 fb^{-1} of Run 2 data [100] employed the $H \rightarrow \gamma\gamma$ and multilepton final states, as well as the final state $H \rightarrow b\bar{b}$ in the VH production mode with the single-lepton decay of the associated boson. The multilepton analysis uses simpler techniques than those previously described [97,99], and trained multivariate methods with tH processes as the signal. The $H \rightarrow \gamma\gamma$ analysis reinterprets the content of the $t\bar{t}H$ categories of a previous analysis. The $H \rightarrow b\bar{b}$ analysis brings little sensitivity and will not be described here. The combined measurement results in an observed limit on the cross-section for the tH production of 1.94 pb at 95% CL in the SM hypothesis. The results for the hypotheses with negative top quark Yukawa coupling are also reported. In commemoration of the 10th anniversary of the Higgs boson discovery,

grand combinations were performed by both CMS [101] and ATLAS [102], including many final states. Categories specifically targeting the tH processes are taken from the $H \rightarrow \gamma\gamma$ channel by ATLAS, and $H \rightarrow \gamma\gamma$ and the multilepton channel at CMS. The CMS combination reports a measured signal strength of $\mu_{tH} = 6.05^{+2.66}_{-2.42}$.

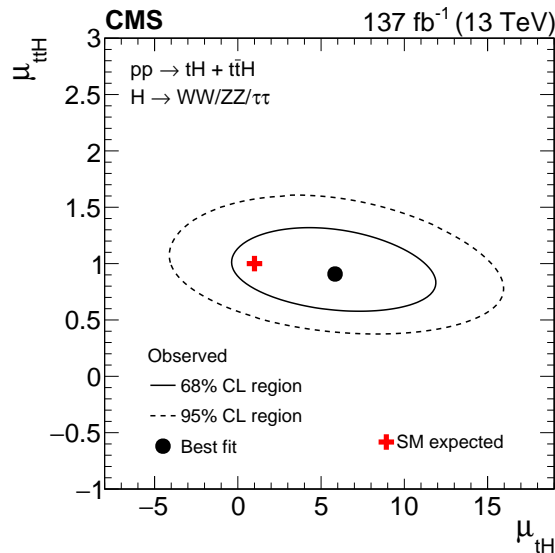


Figure 24. Likelihood contour as a function of the signal strengths for $t\bar{t}H$ and tH processes in the multilepton analysis [99].

Studies estimating the sensitivity to the tH processes at the HL-LHC were expecting a relative uncertainty of 90% on the tH signal strength in the SM hypothesis [103] (with the $t\bar{t}H$ signal strength floating); however, these studies were based on early projections and would need to be updated with the latest ATLAS and CMS results.

3.3.3. Probing the Sign of the Top Quark Yukawa Coupling

With the analyses from ATLAS and CMS for $H \rightarrow \gamma\gamma$ final state [96,97], combined with the CMS multilepton analysis [99] and the earlier CMS combination [100]—all of which include categories that specifically target the tH processes—it is now feasible to determine the sign of the top quark Yukawa coupling, thanks to the interference observed between Feynman diagrams that showcase the Higgs boson coupling to both the top quark and the W boson. The modifier κ_t of the top quark Yukawa coupling in the SM, $y_{t,SM}$, is defined as $\kappa_t = y_t / y_{t,SM}$. Furthermore, since a similar interference is also present in the $H \rightarrow \gamma\gamma$ decay between the top quark loop and the W boson loop, further sensitivity is gained in this channel. Sensitivity to the positive values remains dominated by the $t\bar{t}H$ process in direct measurements, and by the $gg \rightarrow H$ process (involving a top quark loop) in indirect measurements because of the larger cross-section.

Figure 25 shows the likelihood fit value as a function of the κ_t parameter. The best-fit value is positive and close to 1, while a second minimum of the likelihood is found at a value close to -1. As shown on the left side of Figure 25, including the parameterization of the gluon fusion mechanism as a function of κ_t in the likelihood provides more weight to the positive value of κ_t . On the contrary, when only the tH and $t\bar{t}H$ processes are included, more sensitivity is gained on the sign of κ_t . Values outside of $0.65 < \kappa_t < 1.25$ in the first case and $0.87 < \kappa_t < 1.20$ in the second case are excluded at 95% CL by the $H \rightarrow \gamma\gamma$ analysis by ATLAS. The CMS multilepton analysis results in $-0.9 < \kappa_t < -0.7$ or $0.7 < \kappa_t < 1.1$ at 95% CL.

Projections for the measurement of the top quark Yukawa coupling at the HL-LHC are reported by CMS [101] without emphasis on a possible negative coupling. A precision on the order of 3–4% on κ_t would be achievable, while a precision on the order of 10% is achieved today [101,102].

The tH processes, together with the $t\bar{t}H$ process, can also be used to set constraints on a CP-odd top quark Yukawa coupling. Such measurements were performed by ATLAS with the $H \rightarrow \gamma\gamma$ [104] and $H \rightarrow b\bar{b}$ [105] channels, and at CMS with the $H \rightarrow \gamma\gamma$ [106] and multilepton [107] channels. Since the $t\bar{t}H$ process has a larger cross-section than the tH processes, most of the sensitivity will come from the former, and these measurements will not be described here.

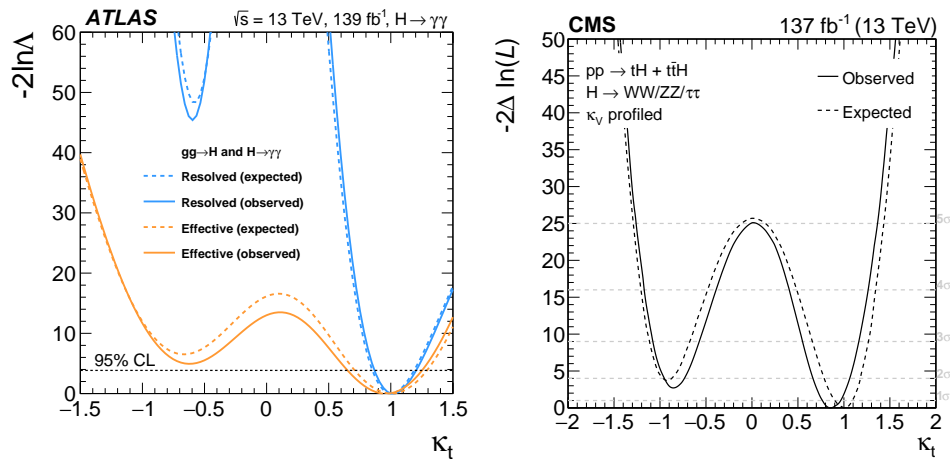


Figure 25. Log-likelihood as a function of the κ_t parameter, in the ATLAS $H \rightarrow \gamma\gamma$ analysis [96] (left), and in the CMS multilepton analysis [99] (right).

4. Discovery Potential of Property Measurements and Interpretations

The large number of single-top events produced at the LHC and the high precision obtained in single-top measurements allow for the measurements of top quark properties, which can be seen as tests of the SM or a search for physics beyond the SM. Although single-top quark production has a lower cross-section compared to $t\bar{t}$ production, the production and subsequent decay of single-top quarks to Wb engage the Wtb vertex twice, during both the top quark production and its decay. This interesting feature can be used to measure several interconnected properties: the couplings of the Wtb vertex, including the CKM matrix element $|V_{tb}|$, the W polarization, and the top quark polarization. Precision measurements of the Wtb couplings can be expressed in terms of CP-even and CP-odd effective couplings or within the EFT. Apart from the $|V_{tb}|$ measurement, which can be inferred from the single-top cross-section, the general experimental strategy for measuring all other properties consists of performing various angular analyses of the top quark decay, and choosing suitable angular distributions to measure the parameters of interest. Additional couplings can be probed within the EFT, including four-fermion couplings, and couplings between the top quark and neutral bosons.

This review will not discuss the top quark mass measurement using the single-top t -channel or the CPT symmetry tests comparing top and antitop quark masses in single-top events (for a recent result, see [108]), since the precision is not yet at the required level for competing with $t\bar{t}$ measurements. This section will cover the other above-mentioned top quark properties using the single-top quark as a probe, reaching a precision similar to or better than that achieved in $t\bar{t}$ measurements.

4.1. Measurement of the CKM Matrix Element $|V_{tb}|$

Because the V_{tb} CKM matrix element is close to unity in the SM, the measurement of V_{tb} is particularly intriguing, and its study is an excellent way to better understand the SM and search for signs of new physics. The measurement of the V_{tb} CKM matrix element is strongly related to the electroweak nature of the single-top production. The cross-section for the single-top production can be used to test the unitarity of the CKM matrix. Assuming

the values of $|V_{td}|$ and $|V_{ts}|$ are much smaller than those of $|V_{tb}|$, the measured single-top cross-section can be used to determine $|V_{tb}|$ according to the following formula [40]:

$$|f_{LV} V_{tb}| = \sqrt{\frac{\sigma^{meas}}{\sigma^{theo}}}, \quad (4)$$

with σ^{meas} denoting the measured cross-section, σ^{th} denoting the SM theoretical cross-section, assuming $|V_{tb}| = 1$, and f_{LV} denoting an anomalous form factor (of the kind vectorial left-handed, as in the SM), which can be different from 1 in new physics models. Such a method was used to reinterpret several single-top cross-sections at 7 and 8 TeV. Their combinations, including ATLAS and CMS results for t -channel, tW production, and s -channel, were performed in the context of the LHCtopWG, leading to the most precise $|f_{LV} V_{tb}|$ measurement to date, as shown in Figure 26. One can see that the t -channel measurements dominate the combination. The latest t -channel measurement at 13 TeV [38] improves over this combination by approximately 30% in precision, with $|V_{tb}| = 1.014 \pm 0.031$ reported.

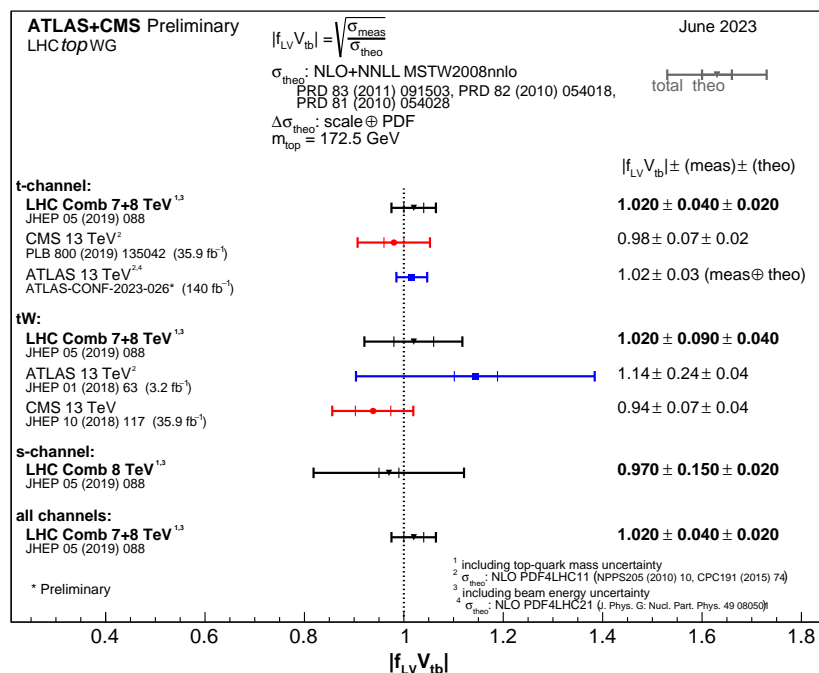


Figure 26. Summary of the ATLAS and CMS extractions of the CKM matrix element V_{tb} from single-top quark measurements [40], compared with theoretical predictions at NLO+NNLL accuracy [71,109,110].

It is possible to release the assumption that $|V_{td}|$ and $|V_{ts}|$ are negligible compared to $|V_{tb}|$. Such a method has also been pursued, consisting of measuring $|V_{tb}|$, $|V_{td}|$ and $|V_{ts}|$ in a model-independent way, using single-top t -channel-enriched events [111]. The main principle of the analysis relies on considering several single-top t -channel signals, according to the presence of a tWb vertex in single-top production ($ST_{b,q}$), in top quark decay ($ST_{q,b}$), or in both ($ST_{b,b}$). Several signal regions, based on the jet and b-tagged jet multiplicities, can be defined and fitted simultaneously. Further discrimination between $ST_{b,q}$, $ST_{q,b}$, and $ST_{b,b}$ is obtained using kinematic and angular properties of the involved processes, using the fact that (1) PDFs are different for each of them, and (2) the presence of an additional b-jet from gluon-splitting can affect top quark reconstruction. Using the constraint of CKM unitarity ($|V_{tb}|^2 + |V_{ts}|^2 + |V_{td}|^2 = 1$), a precision similar to that of the combination [40] is achieved [111] with an integrated luminosity of 35.9 fb^{-1} of 13 TeV proton–proton collisions. The method allows performing the measurements under the constraints of BSM scenarios. The results are compatible with previous measurements and the SM predictions.

4.2. W Boson Polarization Fractions

The V-A structure of the electroweak theory, together with the mass of the particles involved, determine the fractions of longitudinal, left-handed, and right-handed W boson polarization (sometimes called helicity fractions), denoted, respectively, as F_0 , F_L , and F_R . Predictions for these fractions computed at NNLO in pQCD are [112] $F_0 = 0.687 \pm 0.005$, $F_L = 0.311 \pm 0.005$, and $F_R = 0.0017 \pm 0.0001$. Experimentally, the fractions can be measured within the W rest frame where the W boson arises from leptonic top decay, using the angle θ^* , defined as the angle between the direction of the charged lepton and the reversed direction of the b-quark. The differential decay rate is:

$$\frac{1}{\Gamma} \frac{d\Gamma}{dcos\theta^*} = \frac{3}{4}(1 - cos^2\theta^*)F_0 + \frac{3}{8}(1 - cos\theta^*)^2F_L + \frac{3}{8}(1 + cos\theta^*)^2F_R, \quad (5)$$

with $F_0 + F_L + F_R = 1$. The differential decay rate as a function of $cos\theta^*$ is illustrated in Figure 27.

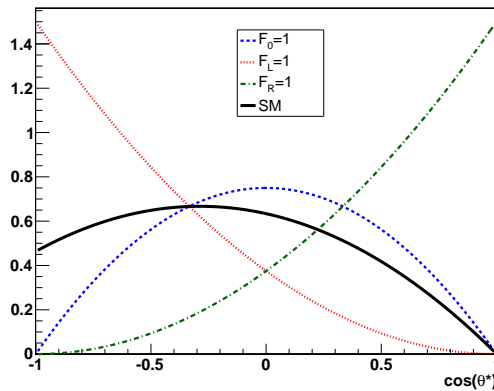


Figure 27. The differential decay rate as a function of $cos\theta^*$ in several scenarios for W boson polarization [113].

The fractions are obtained from a fit of the $cos\theta^*$ distribution to the data. The W boson polarization fractions have been measured at CDF and D0 [114] with a precision on F_0 of the order of 10–15%, using $t\bar{t}$ decay. At the LHC, the single-top production in the t -channel and its large cross-section offer the possibility of measuring the polarization fractions in single-top decay in addition to $t\bar{t}$ decay. The fractions were measured at 8 TeV with CMS [115], as $F_L = 0.298 \pm 0.028(stat) \pm 0.032(syst)$, $F_0 = 0.720 \pm 0.039(stat) \pm 0.037(syst)$, and $F_R = -0.018 \pm 0.019(stat) \pm 0.011(syst)$. The precision achieved with single-top measurements justifies its inclusion in ATLAS and CMS combination of 8 TeV results [116], leading to $F_0 = 0.693 \pm 0.014$, $F_L = 0.315 \pm 0.011$, and $F_R = -0.008 \pm 0.007$. The 7 TeV results were obtained by analyzing $t\bar{t}$ and were not considered since they were expected to bring about negligible improvement.

ATLAS also employed the “generalized helicity fractions and phases” formalism [117] by the means of amplitude decomposition in several angular distributions in the top quark rest frame. Among the parameters measured, the transverse polarization fraction using single-top, and decaying at 7 and 8 TeV [118,119], yields $F_T = F_L + F_R = 0.30 \pm 0.05$ [119] as the best result. ATLAS also measures the phase between amplitudes for longitudinally and transverse W bosons recoiling against left-handed b-quarks [118,119], providing no sign of CP violation. From this formalism, left- and right-handed fractions could in principle be calculated.

4.3. Wtb Effective Couplings and Interpretation in the SM EFT

The Wtb effective couplings were also measured, either at CMS (as extracted from the W boson polarization fractions [115] or measured directly [120]) or by ATLAS, by analyz-

ing the single-top amplitudes [118,119] or measuring various angular asymmetries [121]. The Lagrangian describing the Wtb -effective couplings reads [122]:

$$L_{Wtb} = -\frac{g}{\sqrt{2}} \bar{b} \gamma^\mu (V_L P_L + V_R P_R) t W_\mu^- - \frac{g}{\sqrt{2}} \bar{b} \frac{i \sigma^{\mu\nu} q_\nu}{m_W} (g_L P_L + g_R P_R) t W_\mu^- + h.c. \quad (6)$$

where V_L, V_R denote the vectorial left-handed and right-handed Wtb couplings, and g_L, g_R denote the tensorial left-handed and right-handed Wtb couplings (sometimes called, respectively, $f_V^L, f_V^R, f_T^L, f_T^R$, depending on the convention [120]). In the SM at the LO in pQCD, $V_L = V_{tb}$ while $V_R = g_L = g_R = 0$. The couplings V_R, g_L, g_R are complex and can be CP-odd if their imaginary part is non-zero. The V_{tb} CKM matrix element is inferred from the single-top cross-section measurement, as discussed in Section 4.1.

The analyses have moderate sensitivity to the right-handed vectorial coupling and left-handed tensorial coupling. With a simultaneous fit of both parameters, ATLAS reports $|V_R/V_L| < 0.37$ and $|g_L/V_L| < 0.29$ at 95% CL [119], and CMS reports $f_V^R < 0.16$ and $f_T^L < 0.057$ at 95% CL [120], including f_V^L in the fit using inclusive cross-section information. The best sensitivity on the Wtb couplings is obtained on the g_R coefficient. ATLAS obtained with a simultaneous fit $-0.12 < Re(g_R/V_L) < 0.17$ and $-0.07 < Im(g_R/V_L) < 0.06$ at 95% CL [119]. If using single-top cross-section information and assuming a null imaginary part, CMS obtains $|Re(f_T^R)| < 0.046$. These results can be compared with the combination of an 8 TeV W boson polarization fraction (including $t\bar{t}$ channels) [116]: $-0.11 < Re(V_R) < 0.15$, $-0.08 < Re(g_L) < 0.05$, and $-0.04 < Re(g_R) < 0.02$. Since the imaginary part of g_R cannot be accessed easily from the $t\bar{t}$ process and would need a dedicated analysis [122], the single-top measurements, such as [118,119], are irreplaceable.

The results obtained in the effective coupling formalism can be translated into the modern framework of the SM EFT [123], adding all operators to the SM Lagrangian and respecting gauge invariance. The Wtb couplings considered in Equation (6) (V_L, V_R, g_L, g_R) are, respectively, related to the following four dimension-6 operators:

$$O_{\phi q}^{(3)} = \frac{c_{\phi q}^{(3)}}{\Lambda^2} i(\phi^\dagger \overleftrightarrow{D}_\mu^I \phi)(\bar{q} \gamma^\mu \tau^I q), \quad (7)$$

$$O_{\phi tb} = \frac{c_{\phi tb}}{\Lambda^2} (\phi^\dagger \overleftrightarrow{D}_\mu^I \phi)(\bar{t} \gamma^\mu \tau^I b), \quad (8)$$

$$O_{tW} = \frac{c_{tW}}{\Lambda^2} (\bar{q} \sigma^{\mu\nu} \tau^I t) \tilde{\phi} W_{\mu\nu}^I, \quad (9)$$

$$O_{bW} = \frac{c_{bW}}{\Lambda^2} (\bar{q} \sigma^{\mu\nu} \tau^I b) \phi W_{\mu\nu}^I, \quad (10)$$

using notations from [124]. Results from the combination of the W boson polarization at 8 TeV are [116]: $-3.48 < Re(c_{\phi tb}) < 5.16$, $-0.48 < Re(c_{tW}) < 0.29$, and $-0.96 < Re(c_{bW}) < 0.67$. A translation from the best measurement of $Im(g_R)$ [119] to the EFT formalism using [123] gives $-0.82 < Im(c_{bW}) < 0.70$.

4.4. Top Quark Polarization

Recently, via an analysis of the top quark polarization, ATLAS directly measured the coefficient $Im(c_{tW})$ for the first time [125], using the full Run 2 dataset at 13 TeV. Because of parity conservation in QCD, top quarks in $t\bar{t}$ production are unpolarized, while top quarks are mostly polarized in single-top production. The polarization vector \vec{P} is defined with components $P_i = 2 < S_i >$, where S_i is the top quark spin along the i direction [126], in the top quark rest frame, where the z' direction is defined as the W boson direction, the x' direction is defined as the spectator quark direction projected on the transverse plane, and the y' axis completes the direct basis. On this basis, the values of the polarization vectors are close to $(-0.024, 0, 0.965)$ for the top quark and $(-0.073, 0, -0.957)$ for top antiquark

produced in the t -channel at NNLO in pQCD [125]. The top quark polarization can be extracted from angular distributions of top decay products defined in the top quark rest frame, given by the following general formula:

$$\frac{1}{\Gamma} \frac{d\Gamma}{dcos\theta_X} = \frac{1}{2}(1 + \alpha_X P_X cos\theta_X), \quad (11)$$

where θ_X is the angle between the top quark spin axis and the direction of motion of the chosen decay X , α_X is the spin analyzing power associated with the X , and P_X is the top quark degree of polarization along the direction of X . The measurement of top quark polarization in [125] is performed using the angular distributions related to the charged lepton (shown to have the largest spin analyzing power, close to 1) arising from the top decay and projected in the previously defined directions. If the top quark polarization had previously been measured at the LHC along the z direction (for instance in [121]), the measurement [125] is the most precise and includes x' and y' directions. For top and antitop quarks, it leads, respectively, to $P'_x = 0.01 \pm 0.18$, $P'_y = -0.029 \pm 0.027$, $P'_z = 0.91 \pm 0.10$, and $P'_x = -0.02 \pm 0.20$, $P'_y = -0.007 \pm 0.051$, $P'_z = -0.79 \pm 0.16$. The polarizations along directions x' and z' are also reported in Figure 28. Using the same angular distributions, ATLAS reports $-0.9 < Re(c_{tW}) < 1.4$ and $-0.8 < Im(c_{tW}) < 0.2$ at 95% CL.

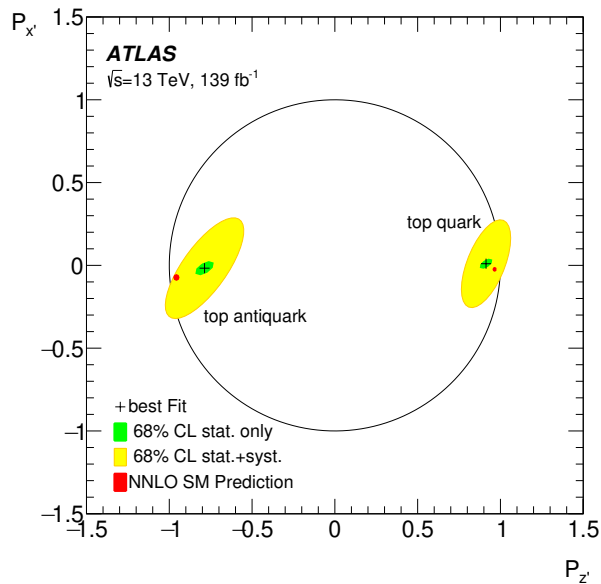


Figure 28. Top quark polarization in the single-top t -channel production along x' and z' directions for the top and antitop quarks [125].

4.5. Discussion on other Couplings with Single-Top Quark Measurements in the SM EFT

If anomalous coupling measurements in single-top quark processes are primarily interesting for Wtb couplings, other couplings are also actively measured, e.g., the coupling between heavy quarks and light quarks, the coupling between heavy quarks and neutral bosons, and the coupling between heavy quarks and leptons. The discussion in this section excludes the FCNC (for a review, see [52]).

In general, single-top production with a boson can help constrain the coupling between top quarks and neutral bosons. The top-Z (resp. top-Higgs) coupling impacts the single-top quark produced in association with a Z boson (resp., a Higgs boson). The top-gluon coupling impacts the tW channel (since tW channel LO diagrams feature one gluon in the initial state) and any production channel considered at NLO, where gluons can be emitted from top quarks. The process of single-top production accompanied by a photon has just been observed and could be used in the near future for measuring the top- γ coupling [82]. It has also been emphasized that the tZq and tHq processes can be greatly impacted by some

of these couplings [127]. However, the cross-sections for processes of single-top production in association with bosons ($t + V$) are lower than those of top pairs produced in association with bosons ($t\bar{t} + V$); therefore, analyses of $t + V$ final states are generally swamped by $t\bar{t} + V$ backgrounds. As a consequence, measuring the tZ , tH , and tg couplings requires, for consistency, the modeling of the anomalous couplings in $t + V$ and $t\bar{t} + V$ simulation samples, which will help in constraining the couplings. It is difficult to disentangle what is the exact contribution of single-top production to the sensitivity in these couplings. We will, therefore, limit ourselves to providing some examples, where the contributions of single-top processes are explicitly included. Generic searches for measuring top quark couplings in the multi-lepton lepton final state define many event classes, targeting a great number of EFT operators that impact tZq and tHq processes [128], e.g., nine operators involving two quarks and one or more bosons (with some impacting the Wtb vertex considered at the production level only), as well as seven operators involving two heavy quarks and two leptons. An updated analysis [129] involving more operators needs to be published. The top gluon coupling was considered in [128] by including its impact on gluon radiation at LO. Measurements of EFT operators in $t\bar{t}Z + tZq$ final states [130] include five operators involving two quarks and one or more bosons (including Wtb vertex) and uses machine learning to maximize sensitivity. The Yukawa coupling is measured in $t\bar{t}H$ analyses by including its impact on tHq , as discussed in Section 3.3.

A recent measurement of the t -channel process using full Run 2 data by ATLAS [38] (to be published) sets constraints on the coupling between light and heavy quarks (the $C_{q,Q}^{(1,3)}$ coefficient within the SMEFT framework), in a competitive manner with global fits reinterpreting LHC data.

The EFT is a consistent framework-preserving gauge invariance in a model-independent way [131] (as long as new physics appears at a high energy scale); therefore, there is a tendency to employ the EFT framework more widely, replacing previous anomalous coupling frameworks. The LHCtopWG, together with the LHC EFT WG, are working on prescriptions toward the combination of direct top quark EFT measurements.

5. Conclusions

After more than 10 years of data-taking with the LHC, the understanding of the physics involving single-top quark processes has undergone a spectacular change. Prior to the LHC, a single-top production was discovered, singling out the t - and s -channels. Nowadays, 14 years on, the differential cross-sections for the t -channel and tW production modes are measured in great detail. The t -channel is routinely used for top quark property measurements. This ranges from the structure of the Wtb vertex to the W boson and top quark polarization, not to mention the top quark mass measurement. The tW production is employed to probe delicate interference effects with the $t\bar{t}$ process. The s -channel process remains to be observed at the LHC, but initial evidence suggests that such an observation is on the horizon. The cross-sections measured for single-top quark production in the t -channel, tW channel, and s -channel by ATLAS and CMS are compared with theoretical predictions in Figure 29.

Run 2 of the LHC offered a new opportunity for observing and exploring the associated production of top quarks and neutral bosons. After its observation, the production of a single-top quark with an associated Z boson was measured differentially for the first time. It is now employed as a probe of various couplings within the SM EFT framework. The associated production with a photon has also been observed with the full Run 2 dataset. The tH processes are used to probe the sign of the top quark Yukawa coupling; however, they have not been observed as yet. The cross-sections measured by ATLAS and CMS for single-top quark production associated with a γ or Z boson are compared with theoretical predictions in Figure 30.

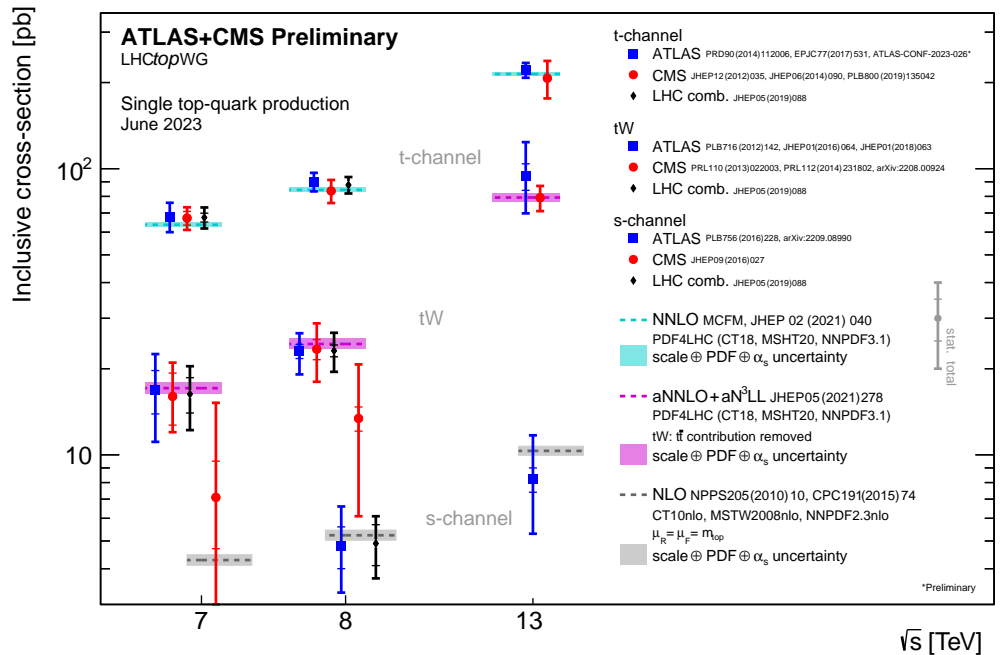


Figure 29. Summary of single-top quark cross-section measurements by ATLAS and CMS in the t -channel, tW production, and s -channel, as functions of the center of mass energy, compared with theoretical predictions at NNLO [11], approximate NNLO+N³LL [12], and NLO [14,132] accuracy, provided by the LHCtopWG [133].

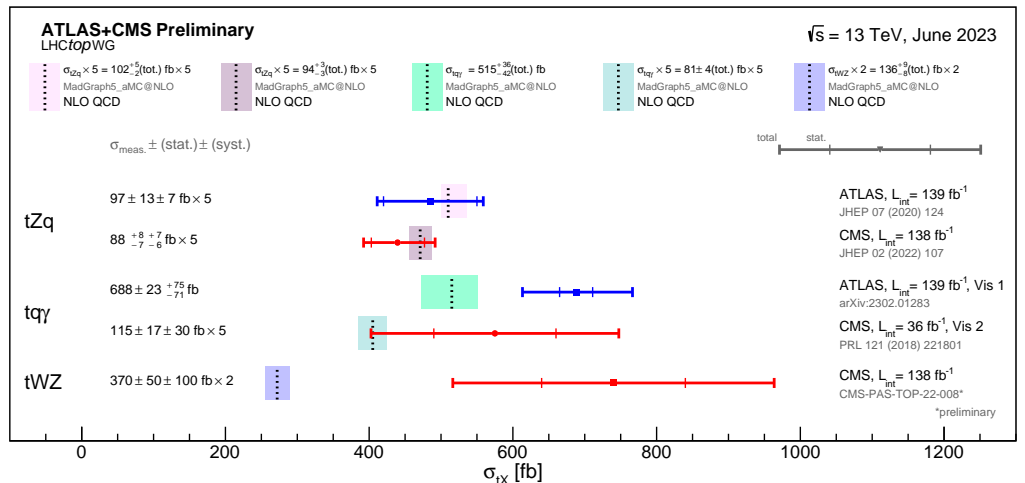


Figure 30. Summary of single-top quark cross-section measurements by ATLAS and CMS in the associated production with a Z boson or a photon compared with theoretical predictions at NLO [78] accuracy; provided by the LHCtopWG [133].

The Run 3 of the LHC is ongoing, with a center-of-mass energy of 13.6 TeV, resulting in a predicted increase of about 11% in the inclusive cross-section relative to 13 TeV for the three main production modes [11,12,77,134] (and a similar increase for the $t\bar{t}$ process [135,136]). One can expect measurements for all of the processes discussed in this review to be performed at this unprecedented energy, verifying if the data still agree with the SM predictions. The luminosity is expected to accumulate during Run 3 in a way that is at least comparable to Run 2, producing a new dataset that is larger by a factor of 1.4 (around 140 fb^{-1} , collected separately by ATLAS and CMS during Run 2, and 200 fb^{-1} during Run 3). Statistically dominated measurements will profit from this step in center-of-mass energy and expected luminosity, such as the measurement of the $t\gamma q$ process, where a first differential cross-section can be targeted. Hopefully, some of the

limitations of the previous measurements will be lifted to improve the precision, provided that additional work on the systematic uncertainties is carried out. For instance, more work is needed on the topic of the parton shower modeling since it is now the largest source of uncertainties in the t -channel measurements and an important source in the measurement of the tW production. Global efforts will also be needed to reduce the systematic uncertainties in the tZq measurement, which is dominated by several sources of large experimental uncertainties. Most of the measurements of the top quark properties in the single-top quark area employ either the t -channel or the tZ production and are impacted by the above uncertainty sources. For the top quark coupling measurements (Wtb vertex and top-boson couplings), it is expected that the movement toward the generalized usage of the EFT will be pursued, allowing the search for new physics in precision measurements in a unified way and allowing for the combination of complementary measurements. Finally, there is hope that the s -channel process could be observed at LHC Run 3 by reducing the uncertainties and refining the analysis techniques. On the other hand, the search for the tH processes will continue, although their observation will have to be postponed to the HL-LHC, where it will remain a challenge [103].

Beyond these extensions of the already engaged single-top quark program, new possibilities can be explored at the HL-LHC. Using boosted top quarks with a jet substructure is one of them (already used for $t\bar{t}$ measurements [137] or in Ref. [90]), since more events will be available in the tails of the distributions to search for new physics [138]. The process of producing three top quarks is occasionally categorized within single-top quark physics. It stands as a minor background in the four top quark process measurements [139,140], and deserves a direct search [141]. The measurement of the tWZ production at Run 2 was the first of its kind, featuring a single-top quark accompanied by two bosons; its observation could be within reach, likely at the HL-LHC, where it could be used to probe the top-boson couplings [142]. And even rarer processes can be reached, i.e., single-top quark production with a combination of two W,Z bosons or photons could be measured beyond tWZ ; some studies suggest that the production of single-top quarks through vector boson fusion is another rare process to explore, offering high sensitivity to new top quark couplings [143]. In general, the program of measuring the top quark couplings within the EFT is still in its infancy. One can foresee that the couplings in which the single-top quark area is relevant will be measured systematically at the HL-LHC [144]. For instance, searching for a possible CP violation in the top-Higgs boson coupling will be conducted, where separating tH from $t\bar{t}H$ will be crucial [145], or measuring the top quark couplings to the gauge bosons, such as the top- γ coupling [82]. Combining measurements from other top quark production modes, along with insights from B physics, electroweak, and Higgs boson measurements, will certainly be essential, and could lead to the observation of statistical deviations indicative of physics beyond the SM.

Author Contributions: Writing—review and editing, J.A. and N.C. All authors have read and agreed to the published version of the manuscript.

Funding: This research received no external funding.

Data Availability Statement: No new data were created or analyzed in this study. Data sharing is not applicable to this review.

Conflicts of Interest: The authors declare no conflict of interest.

References

1. CDF Collaboration. Observation of top quark production in $\bar{p}p$ collisions. *Phys. Rev. Lett.* **1995**, *74*, 2626–2631. [[CrossRef](#)] [[PubMed](#)]
2. D0 Collaboration. Observation of the top quark. *Phys. Rev. Lett.* **1995**, *74*, 2632–2637. [[CrossRef](#)] [[PubMed](#)]
3. D0 Collaboration. Observation of Single Top Quark Production. *Phys. Rev. Lett.* **2009**, *103*, 092001. [[CrossRef](#)] [[PubMed](#)]
4. CDF Collaboration. First Observation of Electroweak Single Top Quark Production. *Phys. Rev. Lett.* **2009**, *103*, 092002. [[CrossRef](#)]
5. D0 Collaboration. Model-independent measurement of t -channel single top quark production in $p\bar{p}$ collisions at $\sqrt{s} = 1.96$ TeV. *Phys. Lett. B* **2011**, *705*, 313–319. [[CrossRef](#)]

6. D0 Collaboration. Evidence for S-Channel Single Top Quark Production in $p\bar{p}$ Collisions at $\sqrt{s} = 1.96$ TeV. *Phys. Lett. B* **2013**, *726*, 656–664. [[CrossRef](#)]
7. CDF Collaboration. Updated Measurement of the Single Top Quark Production Cross Section and Vtb in the Missing Transverse Energy Plus Jets Topology in $p\bar{p}$ Collisions at $\sqrt{s} = 1.96$ TeV. *Phys. Rev. D* **2016**, *93*, 032011. [[CrossRef](#)]
8. CDF Collaboration; D0 Collaboration. Observation of s-channel production of single top quarks at the Tevatron. *Phys. Rev. Lett.* **2014**, *112*, 231803. [[CrossRef](#)]
9. ATLAS Collaboration. Evidence for single top-quark production in the s-channel in proton-proton collisions at $\sqrt{s} = 8$ TeV with the ATLAS detector using the Matrix Element Method. *Phys. Lett. B* **2016**, *756*, 228–246. [[CrossRef](#)]
10. ATLAS Collaboration. Measurement of single top-quark production in the s-channel in proton–proton collisions at $\sqrt{s} = 13$ TeV with the ATLAS detector. *J. High Energy Phys.* **2023**, *6*, 191. [[CrossRef](#)]
11. Campbell, J.; Neumann, T.; Sullivan, Z. Single-top-quark production in the t-channel at NNLO. *J. High Energy Phys.* **2021**, *2*, 40. [[CrossRef](#)]
12. Kidonakis, N.; Yamanaka, N. Higher-order corrections for tW production at high-energy hadron colliders. *J. High Energy Phys.* **2021**, *5*, 278. [[CrossRef](#)]
13. Aliev, M.; Lacker, H.; Langenfeld, U.; Moch, S.; Uwer, P.; Wiedermann, M. HATHOR: HAdronic Top and Heavy quarks crOss section calculatoR. *Comput. Phys. Commun.* **2011**, *182*, 1034–1046. [[CrossRef](#)]
14. Kant, P.; Kind, O.M.; Kintscher, T.; Lohse, T.; Martini, T.; Mölbitz, S.; Rieck, P.; Uwer, P. HatHor for single top-quark production: Updated predictions and uncertainty estimates for single top-quark production in hadronic collisions. *Comput. Phys. Commun.* **2015**, *191*, 74–89. [[CrossRef](#)]
15. Giammanco, A. Single top quark production at the LHC. *Rev. Phys.* **2016**, *1*, 1–12. [[CrossRef](#)]
16. Giammanco, A.; Schwienhorst, R. Single top-quark production at the Tevatron and the LHC. *Rev. Mod. Phys.* **2018**, *90*, 035001. [[CrossRef](#)]
17. ATLAS Collaboration. Top Cross Section Summary Plots—June 2023. 2023. Available online: <https://atlas.web.cern.ch/Atlas/GROUPS/PHYSICS/PUBNOTES/ATL-PHYS-PUB-2023-014> (accessed on 24 July 2023).
18. CMS Collaboration. CMS Top Quark Physics Summary Figures. Available online: <https://twiki.cern.ch/twiki/bin/view/CMSPublic/PhysicsResultsTOPSummaryFigures> (accessed on 24 July 2023).
19. Tait, T.M.P.; Yuan, C.P. Single top quark production as a window to physics beyond the standard model. *Phys. Rev. D* **2000**, *63*, 014018.
20. Drueke, E.; Nutter, J.; Schwienhorst, R.; Vignaroli, N.; Walker, D.G.E.; Yu, J.H. Single Top Production as a Probe of Heavy Resonances. *Phys. Rev. D* **2015**, *91*, 054020. [[CrossRef](#)]
21. Burdman, G. Scalars from top condensation models at hadron colliders. *Phys. Rev. Lett.* **1999**, *83*, 2888–2891.
22. Oakes, R.J.; Whisnant, K.; Yang, J.M.; Young, B.L.; Zhang, X. Single top quark production as a probe of R-parity violating SUSY at p p and p anti-p colliders. *Phys. Rev. D* **1998**, *57*, 534–540.
23. Burdman, G.; Dobrescu, B.A.; Ponton, E. Resonances from two universal extra dimensions. *Phys. Rev. D* **2006**, *74*, 075008.
24. Aguilar-Saavedra, J.A. Identifying top partners at LHC. *J. High Energy Phys.* **2009**, *11*, 30. [[CrossRef](#)]
25. Hassanain, B.; March-Russell, J.; Rosa, J.G. On the possibility of light string resonances at the LHC and Tevatron from Randall-Sundrum throats. *J. High Energy Phys.* **2009**, *7*, 77. [[CrossRef](#)]
26. Atwood, D.; Reina, L.; Soni, A. Phenomenology of two Higgs doublet models with flavor changing neutral currents. *Phys. Rev. D* **1997**, *55*, 3156–3176.
27. Cao, J.J.; Eilam, G.; Frank, M.; Hikasa, K.; Liu, G.L.; Turan, I.; Yang, J.M. SUSY-induced FCNC top-quark processes at the large hadron collider. *Phys. Rev. D* **2007**, *75*, 075021.
28. Agashe, K.; Perez, G.; Soni, A. Collider Signals of Top Quark Flavor Violation from a Warped Extra Dimension. *Phys. Rev. D* **2007**, *75*, 015002.
29. Fontes, D.; Mühlleitner, M.; Romão, J.C.; Santos, R.; Silva, J.a.P.; Wittbrodt, J. The C2HDM revisited. *J. High Energy Phys.* **2018**, *2*, 73. [[CrossRef](#)]
30. Bi, X.J.; Dai, Y.B. CP violation in semileptonic decays of the top quark within MSSM. *Eur. Phys. J. C* **2000**, *12*, 125–135.
31. Behr, J.K.; Grohsjean, A. Dark Matter Searches with Top Quarks. *Universe* **2023**, *9*, 16. [[CrossRef](#)]
32. CMS Collaboration. Measurement of differential cross sections and charge ratios for t-channel single top quark production in proton–proton collisions at $\sqrt{s} = 13$ TeV. *Eur. Phys. J. C* **2020**, *80*, 370. [[CrossRef](#)]
33. CMS Collaboration. Measurement of the t-channel single top quark production cross section in pp collisions at $\sqrt{s} = 7$ TeV. *Phys. Rev. Lett.* **2011**, *107*, 091802. [[CrossRef](#)] [[PubMed](#)]
34. ATLAS Collaboration. Measurement of the t-channel single top-quark production cross section in pp collisions at $\sqrt{s} = 7$ TeV with the ATLAS detector. *Phys. Lett. B* **2012**, *717*, 330–350. [[CrossRef](#)]
35. CMS Collaboration. Measurement of the Single-Top-Quark t-Channel Cross Section in pp Collisions at $\sqrt{s} = 7$ TeV. *J. High Energy Phys.* **2012**, *12*, 35. [[CrossRef](#)]
36. Cowan, G.; Cranmer, K.; Gross, E.; Vitells, O. Asymptotic formulae for likelihood-based tests of new physics. *Eur. Phys. J. C* **2011**, *71*, 1554; Erratum in *Eur. Phys. J. C* **2013**, *73*, 2501. [[CrossRef](#)]

37. ATLAS Collaboration, CMS Collaboration, and the LHC Higgs Combination Group. Procedure for the LHC Higgs Boson Search Combination in Summer 2011. *CMS-NOTE-2011-005, ATL-PHYS-PUB-2011-11*. Available online: <https://cds.cern.ch/record/1379837> (accessed on 24 July 2023).
38. ATLAS Collaboration. Measurement of t -Channel Production of Single Top Quarks and Antiquarks in pp Collisions at 13 TeV Using the Full ATLAS Run 2 Dataset. *ATLAS-CONF-2023-026*. Available online: <https://atlas.web.cern.ch/Atlas/GROUPS/PHYSICS/CONFNOTES/ATLAS-CONF-2023-026> (accessed on 24 July 2023).
39. ATLAS Collaboration. Measurement of t -Channel Single-Top-Quark Production in pp Collisions at $\sqrt{s} = 5.02$ TeV with the ATLAS Detector. *ATLAS-CONF-2023-033*. Available online: <https://atlas.web.cern.ch/Atlas/GROUPS/PHYSICS/CONFNOTES/ATLAS-CONF-2023-033> (accessed on 24 July 2023).
40. ATLAS Collaboration; CMS Collaboration. Combinations of Single-Top-Quark Production Cross-Section Measurements and $|f_{LV}V_{tb}|$ Determinations at $\sqrt{s} = 7$ and 8 TeV with the ATLAS and CMS Experiments. *J. High Energy Phys.* **2019**, *5*, 88. [CrossRef]
41. CMS Collaboration. Measurement of the single top quark and antiquark production cross sections in the t channel and their ratio in proton-proton collisions at $\sqrt{s} = 13$ TeV. *Phys. Lett. B* **2020**, *800*, 135042. [CrossRef]
42. Fischer, N.; Prestel, S.; Ritzmann, M.; Skands, P. Vincia for Hadron Colliders. *Eur. Phys. J. C* **2016**, *76*, 589. [CrossRef] [PubMed]
43. Dasgupta, M.; Dreyer, F.A.; Hamilton, K.; Monni, P.F.; Salam, G.P.; Soyez, G. Parton showers beyond leading logarithmic accuracy. *Phys. Rev. Lett.* **2020**, *125*, 052002. [CrossRef] [PubMed]
44. Ferrario Ravasio, S.; Hamilton, K.; Karlberg, A.; Salam, G.P.; Scyboz, L.; Soyez, G. A parton shower with higher-logarithmic accuracy for soft emissions. *arXiv* **2023**, arXiv:2307.11142 <https://doi.org/10.48550/arXiv.2307.1114>.
45. Corcella, G.; Franceschini, R.; Kim, D. Fragmentation Uncertainties in Hadronic Observables for Top-quark Mass Measurements. *Nucl. Phys. B* **2018**, *929*, 485–526. [CrossRef]
46. ATLAS Collaboration. Comprehensive measurements of t -channel single top-quark production cross sections at $\sqrt{s} = 7$ TeV with the ATLAS detector. *Phys. Rev. D* **2014**, *90*, 112006, [CrossRef]
47. ATLAS Collaboration. Fiducial, total and differential cross-section measurements of t -channel single top-quark production in pp collisions at 8 TeV using data collected by the ATLAS detector. *Eur. Phys. J. C* **2017**, *77*, 531. [CrossRef]
48. CMS Collaboration. Measurement of the t -channel single-top-quark production cross section and of the $|V_{tb}|$ CKM matrix element in pp collisions at $\sqrt{s} = 8$ TeV. *J. High Energy Phys.* **2014**, *6*, 90. [CrossRef]
49. ATLAS Collaboration. Measurement of the inclusive cross-sections of single top-quark and top-antiquark t -channel production in pp collisions at $\sqrt{s} = 13$ TeV with the ATLAS detector. *J. High Energy Phys.* **2017**, *4*, 86. [CrossRef]
50. Nocera, E.R.; Ubiali, M.; Voisey, C. Single Top Production in PDF fits. *J. High Energy Phys.* **2020**, *5*, 67. [CrossRef]
51. ATLAS Collaboration. Measurement of single top-quark production in association with a W boson in the single-lepton channel at $\sqrt{s} = 8$ TeV with the ATLAS detector. *Eur. Phys. J. C* **2021**, *81*, 720. [CrossRef]
52. Castro, N.F.; Skovpen, K. Flavour-Changing Neutral Scalar Interactions of the Top Quark. *Universe* **2022**, *8*, 609. [CrossRef]
53. White, C.D.; Frixione, S.; Laenen, E.; Maltoni, F. Isolating Wt production at the LHC. *J. High Energy Phys.* **2009**, *11*, 74. [CrossRef]
54. Aguilar-Saavedra, J.A. Single top quark production at LHC with anomalous Wtb couplings. *Nucl. Phys. B* **2008**, *804*, 160–192. [CrossRef]
55. ATLAS Collaboration. Evidence for the associated production of a W boson and a top quark in ATLAS at $\sqrt{s} = 7$ TeV. *Phys. Lett. B* **2012**, *716*, 142–159. [CrossRef]
56. CMS Collaboration. Evidence for Associated Production of a Single Top Quark and W Boson in pp Collisions at $\sqrt{s} = 7$ TeV. *Phys. Rev. Lett.* **2013**, *110*, 022003. [CrossRef] [PubMed]
57. ATLAS Collaboration. Measurement of the production cross-section of a single top quark in association with a W boson at 8 TeV with the ATLAS experiment. *J. High Energy Phys.* **2016**, *1*, 64. [CrossRef]
58. CMS Collaboration. Observation of the associated production of a single top quark and a W boson in pp collisions at $\sqrt{s} = 8$ TeV. *Phys. Rev. Lett.* **2014**, *112*, 231802. [CrossRef]
59. ATLAS Collaboration. Measurement of the cross-section for producing a W boson in association with a single top quark in pp collisions at $\sqrt{s} = 13$ TeV with ATLAS. *J. High Energy Phys.* **2018**, *1*, 63. [CrossRef]
60. CMS Collaboration. Measurement of the production cross section for single top quarks in association with W bosons in proton-proton collisions at $\sqrt{s} = 13$ TeV. *J. High Energy Phys.* **2018**, *10*, 117. [CrossRef]
61. ATLAS Collaboration. Measurement of differential cross-sections of a single top quark produced in association with a W boson at $\sqrt{s} = 13$ TeV with ATLAS. *Eur. Phys. J. C* **2018**, *78*, 186, [CrossRef] [PubMed]
62. CMS Collaboration. Measurement of inclusive and differential cross sections for single top quark production in association with a W boson in proton-proton collisions at $\sqrt{s} = 13$ TeV. *J. High Energy Phys.* **2023**, *7*, 46. [CrossRef]
63. CMS Collaboration. Observation of tW production in the single-lepton channel in pp collisions at $\sqrt{s} = 13$ TeV. *J. High Energy Phys.* **2021**, *11*, 111. [CrossRef]
64. ATLAS Collaboration. Search for the production of single vector-like and excited quarks in the Wt final state in pp collisions at $\sqrt{s} = 8$ TeV with the ATLAS detector. *J. High Energy Phys.* **2016**, *2*, 110. [CrossRef]
65. CMS Collaboration. Search for a heavy resonance decaying into a top quark and a W boson in the lepton+jets final state at $\sqrt{s} = 13$ TeV. *J. High Energy Phys.* **2022**, *4*, 48. [CrossRef]
66. Baur, U.; Spira, M.; Zerwas, P.M. Excited Quark and Lepton Production at Hadron Colliders. *Phys. Rev. D* **1990**, *42*, 815–824. [CrossRef] [PubMed]

67. Brochet, S.; Delaere, C.; François, B.; Lemaître, V.; Mertens, A.; Saggio, A.; Vidal Marono, M.; Wertz, S. MoMEMta, a modular toolkit for the Matrix Element Method at the LHC. *Eur. Phys. J. C* **2019**, *79*, 126. [[CrossRef](#)]
68. ATLAS Collaboration. Probing the quantum interference between singly and doubly resonant top-quark production in pp collisions at $\sqrt{s} = 13$ TeV with the ATLAS detector. *Phys. Rev. Lett.* **2018**, *121*, 152002. [[CrossRef](#)] [[PubMed](#)]
69. Ježo, T.; Lindert, J.M.; Nason, P.; Oleari, C.; Pozzorini, S. An NLO+PS generator for $t\bar{t}$ and Wt production and decay including non-resonant and interference effects. *Eur. Phys. J. C* **2016**, *76*, 691. [[CrossRef](#)]
70. Ježo, T.; Lindert, J.M.; Pozzorini, S. Resonance-aware NLOPS matching for off-shell $t\bar{t} + tW$ production with semileptonic decays. *arXiv* **2023**, arXiv:2307.15653. <https://doi.org/10.48550/arXiv.2307.15653>.
71. Kidonakis, N. NNLL resummation for s-channel single top quark production. *Phys. Rev. D* **2010**, *81*, 054028. [[CrossRef](#)]
72. ATLAS Collaboration. Search for s-channel single top-quark production in proton–proton collisions at $\sqrt{s} = 8$ TeV with the ATLAS detector. *Phys. Lett. B* **2015**, *740*, 118–136. [[CrossRef](#)]
73. Kondo, K. Dynamical Likelihood Method for Reconstruction of Events with Missing Momentum. 1: Method and Toy Models. *J. Phys. Soc. Jap.* **1988**, *57*, 4126–4140. [[CrossRef](#)]
74. D0 Collaboration. A precision measurement of the mass of the top quark. *Nature* **2004**, *429*, 638–642. [[CrossRef](#)]
75. CDF Collaboration. Precision measurement of the top quark mass from dilepton events at CDF II. *Phys. Rev. D* **2007**, *75*, 031105. [[CrossRef](#)]
76. CMS Collaboration. Search for s channel single top quark production in pp collisions at $\sqrt{s} = 7$ and 8 TeV. *J. High Energy Phys.* **2016**, *9*, 27. [[CrossRef](#)]
77. Liu, Z.L.; Gao, J. s-channel single top quark production and decay at next-to-next-to-leading-order in QCD. *Phys. Rev. D* **2018**, *98*, 071501. [[CrossRef](#)]
78. Alwall, J.; Frederix, R.; Frixione, S.; Hirschi, V.; Maltoni, F.; Mattelaer, O.; Shao, H.S.; Stelzer, T.; Torrielli, P.; Zaro, M. The automated computation of tree-level and next-to-leading order differential cross sections, and their matching to parton shower simulations. *J. High Energy Phys.* **2014**, *7*, 79. [[CrossRef](#)]
79. CMS Collaboration. Evidence for the associated production of a single top quark and a photon in proton-proton collisions at $\sqrt{s} = 13$ TeV. *Phys. Rev. Lett.* **2018**, *121*, 221802. [[CrossRef](#)]
80. Kidonakis, N.; Yamanaka, N. QCD corrections in $tq\gamma$ production at hadron colliders. *Eur. Phys. J. C* **2022**, *82*, 670. [[CrossRef](#)]
81. ATLAS Collaboration. Observation of single-top-quark production in association with a photon using the ATLAS detector. *arXiv* **2023**, arXiv:2302.01283.
82. Fael, M.; Gehrman, T. Probing top quark electromagnetic dipole moments in single-top-plus-photon production. *Phys. Rev. D* **2013**, *88*, 033003. [[CrossRef](#)]
83. ATLAS Collaboration. Measurements of inclusive and differential cross-sections of combined $t\bar{t}\gamma$ and $tW\gamma$ production in the $e\mu$ channel at 13 TeV with the ATLAS detector. *J. High Energy Phys.* **2020**, *9*, 49. [[CrossRef](#)]
84. ATLAS Collaboration. Measurement of the production cross-section of a single top quark in association with a Z boson in proton–proton collisions at 13 TeV with the ATLAS detector. *Phys. Lett. B* **2018**, *780*, 557–577. [[CrossRef](#)]
85. CMS Collaboration. Measurement of the associated production of a single top quark and a Z boson in pp collisions at $\sqrt{s} = 13$ TeV. *Phys. Lett. B* **2018**, *779*, 358–384. [[CrossRef](#)]
86. Kidonakis, N.; Yamanaka, N. Soft-gluon corrections for tqZ production. *Phys. Lett. B* **2023**, *838*, 137708. [[CrossRef](#)]
87. CMS Collaboration. Inclusive and differential cross section measurements of single top quark production in association with a Z boson in proton-proton collisions at $\sqrt{s} = 13$ TeV. *J. High Energy Phys.* **2022**, *2*, 107. [[CrossRef](#)]
88. CMS Collaboration. Observation of Single Top Quark Production in Association with a Z Boson in Proton-Proton Collisions at $\sqrt{s} = 13$ TeV. *Phys. Rev. Lett.* **2019**, *122*, 132003. [[CrossRef](#)]
89. ATLAS Collaboration. Observation of the associated production of a top quark and a Z boson in pp collisions at $\sqrt{s} = 13$ TeV with the ATLAS detector. *J. High Energy Phys.* **2020**, *7*, 124. [[CrossRef](#)]
90. CMS Collaboration. Evidence for tWZ Production in Proton-Proton Collisions at $\sqrt{s} = 13$ TeV in Multilepton Final States. CMS-PAS-TOP-22-008. Available online: <https://cms-results.web.cern.ch/cms-results/public-results/preliminary-results/TOP-22-008/index.html> (accessed on 24 July 2023).
91. ATLAS Collaboration. Studies on Top-Quark Monte Carlo Modelling for Top2016. Available online: <https://atlas.web.cern.ch/Atlas/GROUPS/PHYSICS/PUBNOTES/ATL-PHYS-PUB-2016-020/> (accessed on 24 July 2023).
92. LHC Higgs Cross Section Working Group. Handbook of LHC Higgs Cross Sections: 4. Deciphering the Nature of the Higgs Sector. *arXiv* **2016**, arXiv:1610.07922. <https://doi.org/10.23731/CYRM-2017-002>.
93. Forslund, M.; Kidonakis, N. Soft-gluon corrections for the associated production of a single top quark and a Higgs boson. *Phys. Rev. D* **2021**, *104*, 034024. [[CrossRef](#)]
94. CMS Collaboration. Search for the associated production of a Higgs boson with a single top quark in proton-proton collisions at $\sqrt{s} = 8$ TeV. *J. High Energy Phys.* **2016**, *6*, 177. [[CrossRef](#)]
95. Farina, M.; Grojean, C.; Maltoni, F.; Salvioni, E.; Thamm, A. Lifting degeneracies in Higgs couplings using single top production in association with a Higgs boson. *J. High Energy Phys.* **2013**, *5*, 22. [[CrossRef](#)]
96. ATLAS Collaboration. Measurement of the properties of Higgs boson production at $\sqrt{s} = 13$ TeV in the $H \rightarrow \gamma\gamma$ channel using 139 fb^{-1} of pp collision data with the ATLAS experiment. *J. High Energy Phys.* **2023**, *7*, 88. [[CrossRef](#)]

97. CMS Collaboration. Measurements of Higgs boson production cross sections and couplings in the diphoton decay channel at $\sqrt{s} = 13$ TeV. *J. High Energy Phys.* **2021**, *7*, 27. [[CrossRef](#)]
98. Berger, N.; Bertella, C.; Calvet, T.P.; Calvetti, M.; Dao, V.; Delmastro, M.; Duehrssen-Debling, M.; Francavilla, P.; Haddad, Y.; Kivernyk, O.; et al. Simplified Template Cross Sections—Stage 1.1. *arXiv* **2019**, arXiv:1906.02754. <https://doi.org/10.48550/arXiv.1906.02754>.
99. CMS Collaboration. Measurement of the Higgs boson production rate in association with top quarks in final states with electrons, muons, and hadronically decaying tau leptons at $\sqrt{s} = 13$ TeV. *Eur. Phys. J. C* **2021**, *81*, 378. [[CrossRef](#)] [[PubMed](#)]
100. CMS Collaboration. Search for associated production of a Higgs boson and a single top quark in proton-proton collisions at $\sqrt{s} = 13$ TeV. *Phys. Rev. D* **2019**, *99*, 092005. [[CrossRef](#)]
101. CMS Collaboration. A portrait of the Higgs boson by the CMS experiment ten years after the discovery. *Nature* **2022**, *607*, 60–68. [[CrossRef](#)] [[PubMed](#)]
102. ATLAS Collaboration. A detailed map of Higgs boson interactions by the ATLAS experiment ten years after the discovery. *Nature* **2022**, *607*, 52–59; Erratum in *Nature* **2022**, *612*, E24. [[CrossRef](#)] [[PubMed](#)]
103. CMS Collaboration. Sensitivity Projections for Higgs Boson Properties Measurements at the HL-LHC. *CMS-PAS-FTR-18-011*. Available online: <https://cms-results.web.cern.ch/cms-results/public-results/preliminary-results/FTR-18-011/index.html> (accessed on 24 July 2023).
104. ATLAS Collaboration. CP Properties of Higgs Boson Interactions with Top Quarks in the $t\bar{t}H$ and tH Processes Using $H \rightarrow \gamma\gamma$ with the ATLAS Detector. *Phys. Rev. Lett.* **2020**, *125*, 061802, [[CrossRef](#)]
105. ATLAS Collaboration. Probing the CP nature of the top-Higgs Yukawa coupling in $t\bar{t}H$ and tH events with $H \rightarrow b\bar{b}$ decays using the ATLAS detector at the LHC. *arXiv* **2023**, arXiv:2303.05974. <https://doi.org/10.48550/arXiv.2303.05974>.
106. CMS Collaboration. Measurements of $t\bar{t}H$ Production and the CP Structure of the Yukawa Interaction between the Higgs Boson and Top Quark in the Diphoton Decay Channel. *Phys. Rev. Lett.* **2020**, *125*, 061801. [[CrossRef](#)]
107. CMS Collaboration. Search for CP violation in $t\bar{t}H$ and tH production in multilepton channels in proton-proton collisions at $\sqrt{s} = 13$ TeV. *J. High Energy Phys.* **2023**, *7*, 92. [[CrossRef](#)]
108. CMS Collaboration. Measurement of the top quark mass using events with a single reconstructed top quark in pp collisions at $\sqrt{s} = 13$ TeV. *J. High Energy Phys.* **2021**, *12*, 161. [[CrossRef](#)]
109. Kidonakis, N. Next-to-next-to-leading-order collinear and soft gluon corrections for t-channel single top quark production. *Phys. Rev. D* **2011**, *83*, 091503. [[CrossRef](#)]
110. Kidonakis, N. Two-loop soft anomalous dimensions for single top quark associated production with a W^- or H^- . *Phys. Rev. D* **2010**, *82*, 054018. [[CrossRef](#)]
111. CMS Collaboration. Measurement of CKM matrix elements in single top quark t -channel production in proton-proton collisions at $\sqrt{s} = 13$ TeV. *Phys. Lett. B* **2020**, *808*, 135609. [[CrossRef](#)]
112. Czarnecki, A.; Korner, J.G.; Piclum, J.H. Helicity fractions of W bosons from top quark decays at NNLO in QCD. *Phys. Rev. D* **2010**, *81*, 111503. [[CrossRef](#)]
113. CMS Collaboration. Measurement of the W boson helicity fractions in the decays of top quark pairs to lepton + jets final states produced in pp collisions at $\sqrt{s} = 8$ TeV. *Phys. Lett. B* **2016**, *762*, 512–534. [[CrossRef](#)]
114. CDF Collaboration; D0 Collaboration. Combination of CDF and D0 measurements of the W boson helicity in top quark decays. *Phys. Rev. D* **2012**, *85*, 071106, [[CrossRef](#)]
115. CMS Collaboration. Measurement of the W boson helicity in events with a single reconstructed top quark in pp collisions at $\sqrt{s} = 8$ TeV. *J. High Energy Phys.* **2015**, *1*, 53. [[CrossRef](#)]
116. CDF Collaboration; D0 Collaboration. Combination of the W boson polarization measurements in top quark decays using ATLAS and CMS data at $\sqrt{s} = 8$ TeV. *J. High Energy Phys.* **2020**, *8*, 51. [[CrossRef](#)]
117. Boudreau, J.; Escobar, C.; Mueller, J.; Sapp, K.; Su, J. Single top quark differential decay rate formulae including detector effects. *arXiv* **2013**, arXiv:1304.5639. <https://doi.org/10.48550/arXiv.1304.5639>.
118. ATLAS Collaboration. Search for anomalous couplings in the Wtb vertex from the measurement of double differential angular decay rates of single top quarks produced in the t -channel with the ATLAS detector. *J. High Energy Phys.* **2016**, *4*, 23. [[CrossRef](#)]
119. ATLAS Collaboration. Analysis of the Wtb vertex from the measurement of triple-differential angular decay rates of single top quarks produced in the t -channel at $\sqrt{s} = 8$ TeV with the ATLAS detector. *J. High Energy Phys.* **2017**, *12*, 17. [[CrossRef](#)]
120. CMS Collaboration. Search for anomalous Wtb couplings and flavour-changing neutral currents in t-channel single top quark production in pp collisions at $\sqrt{s} = 7$ and 8 TeV. *J. High Energy Phys.* **2017**, *2*, 28. [[CrossRef](#)]
121. ATLAS Collaboration. Probing the $W tb$ vertex structure in t-channel single-top-quark production and decay in pp collisions at $\sqrt{s} = 8$ TeV with the ATLAS detector. *J. High Energy Phys.* **2017**, *4*, 124. [[CrossRef](#)]
122. Aguilar-Saavedra, J.A.; Carvalho, J.; Castro, N.F.; Veloso, F.; Onofre, A. Probing anomalous Wtb couplings in top pair decays. *Eur. Phys. J. C* **2007**, *50*, 519–533.
123. Buckley, A.; Englert, C.; Ferrando, J.; Miller, D.J.; Moore, L.; Russell, M.; White, C.D. Constraining top quark effective theory in the LHC Run II era. *J. High Energy Phys.* **2016**, *4*, 15. [[CrossRef](#)]
124. Grzadkowski, B.; Iskrzynski, M.; Misiak, M.; Rosiek, J. Dimension-Six Terms in the Standard Model Lagrangian. *J. High Energy Phys.* **2010**, *10*, 85. [[CrossRef](#)]

125. ATLAS Collaboration. Measurement of the polarisation of single top quarks and antiquarks produced in the t-channel at $\sqrt{s} = 13$ TeV and bounds on the tWb dipole operator from the ATLAS experiment. *J. High Energy Phys.* **2022**, *11*, 40. [[CrossRef](#)]
126. Aguilar-Saavedra, J.A.; Amor Dos Santos, S. New directions for top quark polarization in the *t*-channel process. *Phys. Rev. D* **2014**, *89*, 114009. [[CrossRef](#)]
127. Degrande, C.; Maltoni, F.; Mimasu, K.; Vryonidou, E.; Zhang, C. Single-top associated production with a Z or H boson at the LHC: The SMEFT interpretation. *J. High Energy Phys.* **2018**, *10*, 5. [[CrossRef](#)]
128. CMS Collaboration. Search for new physics in top quark production with additional leptons in proton-proton collisions at $\sqrt{s} = 13$ TeV using effective field theory. *J. High Energy Phys.* **2021**, *3*, 95. [[CrossRef](#)]
129. CMS Collaboration. Search for physics beyond the standard model in top quark production with additional leptons in the context of effective field theory. *arXiv* **2023**, arXiv:2307.15761. <https://doi.org/10.48550/arXiv.2307.15761>.
130. CMS Collaboration. Probing effective field theory operators in the associated production of top quarks with a Z boson in multilepton final states at $\sqrt{s} = 13$ TeV. *J. High Energy Phys.* **2021**, *12*, 83. [[CrossRef](#)]
131. Degrande, C.; Greiner, N.; Kilian, W.; Mattelaer, O.; Mebane, H.; Stelzer, T.; Willenbrock, S.; Zhang, C. Effective Field Theory: A Modern Approach to Anomalous Couplings. *Ann. Phys.* **2013**, *335*, 21–32. [[CrossRef](#)]
132. Campbell, J.M.; Ellis, R.K. MCFM at the Tevatron and the LHC. *Nucl. Phys. B Proc. Suppl.* **2010**, *205–206*, 10–15. [[CrossRef](#)]
133. LHC Top Working Group. LHCTopWG Summary Plots. Available online: <https://twiki.cern.ch/twiki/bin/view/LHCPhysics/LHCTopWGSummaryPlots> (accessed on 24 July 2023).
134. LHC Top Working Group. Predictions at NNLO of Single Top-Quark Production Cross-Sections. Available online: <https://twiki.cern.ch/twiki/bin/view/LHCPhysics/SingleTopNNLORef> (accessed on 24 July 2023).
135. LHC Top Working Group. NNLO+NNLL Top-Quark-Pair Cross Sections. Available online: <https://twiki.cern.ch/twiki/bin/view/LHCPhysics/TtbarNNLO> (accessed on 24 July 2023).
136. Czakon, M.; Mitov, A. Top++: A Program for the Calculation of the Top-Pair Cross-Section at Hadron Colliders. *Comput. Phys. Commun.* **2014**, *185*, 2930. [[CrossRef](#)]
137. CMS Collaboration. Measurement of differential $t\bar{t}$ production cross sections in the full kinematic range using lepton+jets events from proton-proton collisions at $\sqrt{s} = 13$ TeV. *Phys. Rev. D* **2021**, *104*, 092013. [[CrossRef](#)]
138. Aguilar-Saavedra, J.A.; Mangano, M.L. New physics with boosted single top production at the LHC and future colliders. *Eur. Phys. J. C* **2020**, *80*, 5. [[CrossRef](#)]
139. ATLAS Collaboration. Observation of four-top-quark production in the multilepton final state with the ATLAS detector. *Eur. Phys. J. C* **2023**, *83*, 496. [[CrossRef](#)]
140. CMS Collaboration. Observation of four top quark production in proton-proton collisions at $\sqrt{s} = 13$ TeV. *arXiv* **2023**, arXiv:2305.13439. <https://doi.org/10.48550/arXiv.2305.13439>.
141. Ahmed, I.; Bi, N.; Ather, M.W.; Amjad, M.S. Observability of triple top quark signal at future hadron colliders. *Prog. Theor. Exp. Phys.* **2023**, *2023*, 053B01. [[CrossRef](#)]
142. Faham, H.E.; Maltoni, F.; Mimasu, K.; Zaro, M. Single top production in association with a WZ pair at the LHC in the SMEFT. *J. High Energy Phys.* **2022**, *1*, 100. [[CrossRef](#)]
143. Maltoni, F.; Mantani, L.; Mimasu, K. Top-quark electroweak interactions at high energy. *J. High Energy Phys.* **2019**, *10*, 4. [[CrossRef](#)]
144. Durieux, G.; Camacho, A.G.; Mantani, L.; Miralles, V.; López, M.M.; Llácer Moreno, M.; Poncelet, R.; Vryonidou, E.; Vos, M. Snowmass White Paper: Prospects for the measurement of top-quark couplings. In Proceedings of the Snowmass 2021, Washington, DC, USA, 17–27 July 2022.
145. Bahl, H.; Bechtle, P.; Heinemeyer, S.; Katzy, J.; Klingl, T.; Peters, K.; Sainpert, M.; Stefaniak, T.; Weiglein, G. Indirect \mathcal{CP} probes of the Higgs-top-quark interaction: Current LHC constraints and future opportunities. *J. High Energy Phys.* **2020**, *11*, 127. [[CrossRef](#)]

Disclaimer/Publisher’s Note: The statements, opinions and data contained in all publications are solely those of the individual author(s) and contributor(s) and not of MDPI and/or the editor(s). MDPI and/or the editor(s) disclaim responsibility for any injury to people or property resulting from any ideas, methods, instructions or products referred to in the content.